Cell

Resource

Revealing the Activity of Trimeric G-proteins in Live Cells with a Versatile Biosensor Design

Graphical Abstract

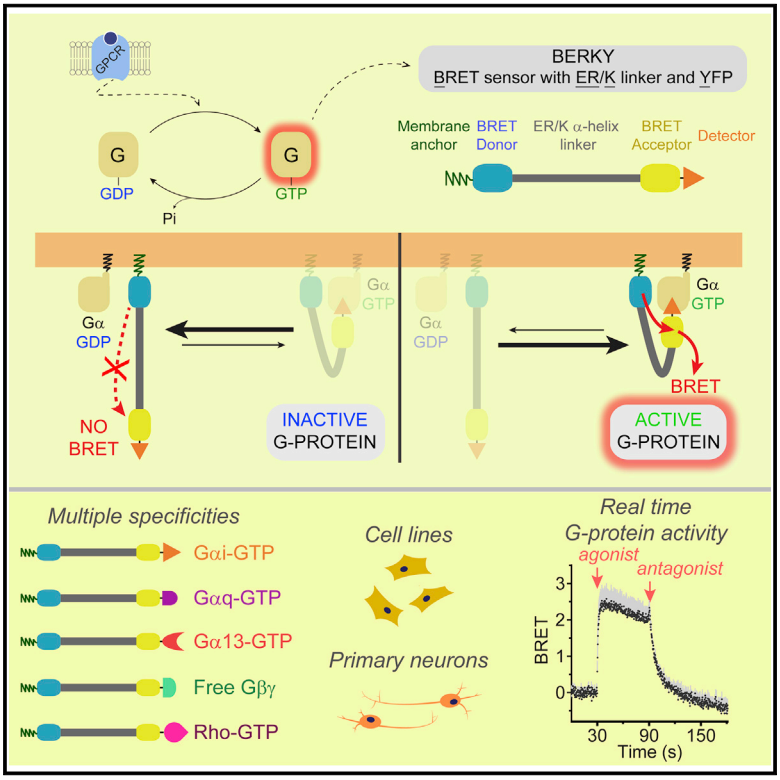

Highlights

- Optical biosensors directly detect active G-proteins in real time in live cells
- Unimolecular sensors report activity of natively expressed GPCRs/G-proteins
- Versatile modular design allows customization for multiple G-protein specificities
- Proof-of-principle implementation for cancer and neurobiology applications

Authors

Marcin Maziarz, Jong-Chan Park, Anthony Leyme, Arthur Marivin, Alberto Garcia-Lopez, Prachi P. Patel, Mikel Garcia-Marcos

Correspondence

mgm1@bu.edu

In Brief

A suite of modular optical biosensors enables detection of G-protein activity in live cells in contexts ranging from tumor cells to primary neurons.

Maziarz et al., 2020, Cell *182*, 1–16
August 6, 2020
https://doi.org/10.1016/j.cell.2020.06.020

CellPress

Please cite this article in press as: Maziarz et al., Revealing the Activity of Trimeric G-proteins in Live Cells with a Versatile Biosensor Design, Cell (2020), https://doi.org/10.1016/j.cell.2020.06.020

Cell

CellPress

Resource

Revealing the Activity of Trimeric G-proteins in Live Cells with a Versatile Biosensor Design

Marcin Maziarz,[1] Jong-Chan Park,[1] Anthony Leyme,[1] Arthur Marivin,[1] Alberto Garcia-Lopez,[1] Prachi P. Patel,[1] and Mikel Garcia-Marcos[1,2,*]

[1]Department of Biochemistry, Boston University School of Medicine, Boston, MA 02118, USA

[2]Lead Contact

*Correspondence: mgm1@bu.edu

https://doi.org/10.1016/j.cell.2020.06.020

SUMMARY

Heterotrimeric G-proteins (Gαβγ) are the main transducers of signals from GPCRs, mediating the action of countless natural stimuli and therapeutic agents. However, there are currently no robust approaches to directly measure the activity of endogenous G-proteins in cells. Here, we describe a suite of optical biosensors that detect endogenous active G-proteins with sub-second resolution in live cells. Using a modular design principle, we developed genetically encoded, unimolecular biosensors for endogenous Gα-GTP and free Gβγ: the two active species of heterotrimeric G-proteins. This design was leveraged to generate biosensors with specificity for different heterotrimeric G-proteins or for other G-proteins, such as Rho GTPases. Versatility was further validated by implementing the biosensors in multiple contexts, from characterizing cancer-associated G-protein mutants to neurotransmitter signaling in primary neurons. Overall, the versatile biosensor design introduced here enables studying the activity of endogenous G-proteins in live cells with high fidelity, temporal resolution, and convenience.

INTRODUCTION

G-protein coupled receptors (GPCRs) are a large family of membrane proteins that initiate cellular responses to a wide range of extracellular signals, like neurotransmitters, hormones, or photons (Gilman, 1987). Consequently, they are critical for many physiological processes, and their dysregulation frequently leads to human disease (Dorsam and Gutkind, 2007; Farfel et al., 1999; Gilman, 1987; O'Hayre et al., 2013), which is also in agreement with the fact that more than 30% of US Food and Drug Administration (FDA)-approved drugs target GPCRs (Sriram and Insel, 2018). The main mechanism of action of GPCRs is through activation of heterotrimeric G-proteins, although mounting evidence indicates that they can also signal by coupling to arrestins (Weis and Kobilka, 2018). The defining event in G-protein activation is the exchange of guanosine diphosphate (GDP) for guanosine triphosphate (GTP) on the Gα subunit of Gαβγ heterotrimers, which is catalyzed by the guanine-nucleotide exchange factor (GEF) activity of ligand-activated GPCRs. A consequence of nucleotide exchange is that Gα-GTP and Gβγ dissociate (or rearrange) so that both become active signaling species competent for engaging their respective effectors. In broad strokes, the specific signaling pathways modulated by Gα-GTP subunits depend on the G-protein family to which they belong ($G_{i/o}$, $G_{q/11}$, $G_{12/13}$, and G_s, based on structural conservation). Signaling is turned off by the intrinsic GTPase activity of Gα, leading to re-association of Gα with Gβγ. In addition, the duration and amplitude of G-protein signaling is controlled by many accessory proteins that bind G-proteins and add layers of complexity to the regulation of their activity (De Vries et al., 2000; Dohlman and Thorner, 1997; Druey et al., 1996; Ross and Wilkie, 2000; Siderovski and Willard, 2005). This includes guanine-nucleotide dissociation inhibitors (GDIs) (Sato et al., 2006; Willard et al., 2004), which bind Gα and lock it in an inactive GDP-bound state, and GTPase-activating proteins (GAPs) (Ross and Wilkie, 2000), which accelerate the rate of GTP hydrolysis by Gα, as well as other regulators, like non-receptor GEFs (Cismowski et al., 2000; DiGiacomo et al., 2018; Garcia-Marcos et al., 2009, 2015; Tall, 2013).

Developing tools to monitor G-protein activity with high fidelity and precision is crucial to elucidate the mode of action of many neurotransmitters, hormones or drugs and to discover novel therapeutic agents. Studying downstream events (e.g., second messengers) as a proxy for G-protein activation has significant caveats because fidelity is compromised by pathway crosstalk and signal amplification events. Historically, the development of ratiometric fluorescence or bioluminescence resonance energy transfer (FRET or BRET, respectively) biosensors allowed more direct, sensitive, and precise measurement of G-protein activity in live cells (Lohse et al., 2012). Early studies showed that fusing FRET or BRET donor/acceptor pairs to Gα and Gβγ enabled detection of GPCR-mediated G-protein activation (Bünemann et al., 2003; Galés et al., 2006; Gibson and Gilman, 2006; Janetopoulos et al., 2001). The rationale behind the design

Please cite this article in press as: Maziarz et al., Revealing the Activity of Trimeric G-proteins in Live Cells with a Versatile Biosensor Design, Cell (2020), https://doi.org/10.1016/j.cell.2020.06.020

of these biosensors is that resonance energy transfer (RET) is highly dependent on the distance and orientation of donor and acceptor molecules so that Gα-Gβγ dissociation and/or rearrangement upon activation leads to changes in FRET or BRET. Another RET biosensor design was introduced later (Hollins et al., 2009), in which activation-induced Gα-Gβγ dissociation was detected using the C-terminal region of GRK3 fused to a RET donor as a separate "detector module" for free Gβγ tagged with a RETacceptor.

Despite the tremendous utility of RET-based biosensors for trimeric G-protein activity developed to date, they still have significant limitations. Current RET-based biosensors can only measure Gα-Gβγ subunit dissociation but not Gα-GTP formation, which would be the most direct readout of the defining event in GPCR-mediated activation; i.e., nucleotide exchange. Although Gα-Gβγ rearrangement and nucleotide exchange on Gα tend to correlate, there are modes of G-protein regulation that cannot be captured by looking at Gα-Gβγ rearrangement alone. For example, GoLoco GDIs are believed to modulate GPCR signaling by blocking Gα-GTP formation while promoting Gα-Gβγ dissociation (Willard et al., 2004), and Ric-8 non-receptor GEFs promote Gα-GTP formation only on monomeric Gα but not on Gα-Gβγ complexes (Tall et al., 2003). Another major caveat is that existing RET-based biosensors require overexpression of exogenous G-proteins (usually tagged with bulky fluorescent or luminescent proteins) to detect their activity, which compromises the fidelity of readouts. In other words, inclusion of G-proteins as integral biosensor components precludes direct assessment of the activity of endogenous G-proteins in their native, physiological environment in the cell. Moreover, these biosensors require simultaneous overexpression of three to four genetic components (Gα, Gβ, Gγ, and, sometimes [Hollins et al., 2009], a detector module), which limits their use to systems in which genetic manipulation is easy. Consequently, the vast majority of work with G-protein biosensors uses easily transfectable cell lines (e.g., HEK293), which are not necessarily relevant for many physiological processes controlled by GPCRs and, in most cases, leading to the need to overexpress exogenous GPCRs. As a consequence, the ultimate goal of translating discoveries regarding the cell biology and pharmacology of GPCR signaling into clinically relevant applications is compromised.

To our knowledge, there is no biosensor capable of detecting endogenous active G-proteins under fully native conditions (e.g., with endogenous GPCRs). We set out to develop RET-based ratiometric biosensors for detecting endogenous, *bona fide* active G-protein species (i.e., Gα-GTP and free Gβγ) in live cells. Here we first described the design of a bi-molecular BRET biosensor that can detect exogenous Gα-GTP species of the $G_{i/o}$ family with high fidelity, specificity, and temporal resolution. Then we converted this Gα-GTP probe into a unimolecular design to demonstrate that a biosensor made of a single genetic component can quantitatively detect activation of endogenously expressed G-proteins without compromising downstream signaling. By leveraging this two-step approach and the modular design of our biosensors, we further developed additional biosensors for endogenous Gα-GTP species of the $G_{q/11}$ or $G_{12/13}$ families, for endogenous free Gβγ, or even for G-proteins not directly coupled to GPCRs. We implemented our suite of biosensors to capture modes of G-protein modulation untractable by preexisting biosensors to define the properties of previously uncharacterized cancer-associated G-protein mutants and to directly detect activation of many endogenous GPCR/G-protein complexes across several cell types, including physiologically relevant models such as primary neuronal cultures.

RESULTS AND DISCUSSION

Direct and Specific Detection of Gαi-GTP

Our first goal was to develop a probe to detect Gα-GTP species as a direct measure of G-protein activity. For this, we sought to identify suitable biosensor components in a bi-molecular BRET format with exogenously expressed G-proteins. We envisioned the design of a bi-molecular BRET-based biosensor for Gαi-GTP inspired by a previously described free Gβγ biosensor (Hollins et al., 2009). A BRET acceptor (yellow fluorescent protein [YFP]) is inserted into Gαi at an internal position that does not compromise activity (helical domain b/c loop) (Gibson and Gilman, 2006), and the BRET donor nanoluciferase (Nluc) (Hall et al., 2012) is fused to a separate detector module with a membrane targeting sequence. We reasoned that the ideal detector module should (1) bind Gαi-GTP but not Gαi-GDP or other Gα proteins to have specificity, (2) bind with high affinity (but reversibly) to be sensitive, and (3) have little or no effect on the activity of the target G-protein to report activity with fidelity (Figure 1A). By mining the literature, we identified the synthetic peptide KB-1753 as a candidate that fulfills all of these criteria (Johnston et al., 2006). KB-1753 binds reversibly to GTP-loaded Gαi1, Gαi2, or Gαi3 (K_d, ~1 μM) but not to Gαi-GDP or other Gα subunits and has no effect on intrinsic nucleotide exchange or hydrolysis by Gαi (Johnston et al., 2006). HEK293T cells co-expressing KB-1753-Nluc and Gαi3-YFP/Gβγ displayed a rapid increase in BRET upon agonist-mediated activation of the GPCR $\alpha2_A$-adrenergic receptor ($\alpha2_A$-AR), which rapidly returned to basal levels upon antagonist addition (Figures 1A and 1B). Agonist dose dependence curves (Figures 1B and 1C) revealed a half-maximal effective concentration (EC_{50}) similar to previously reported values using other readouts or the ligand-receptor binding constant (Harding et al., 2018). Equivalent observations were made with another Gi-coupled GPCR, the μ-opioid receptor (MOR) (Figures S1A and S1B). These results show that the newly designed Gαi-GTP biosensor can detect GPCR-regulated G-protein activity with high fidelity and sensitivity because it captures the characteristic rapid kinetics of G-protein activation/deactivation and agonist potency.

We wondered whether the number of genetic components used for this biosensor design could be reduced by half by eliminating Gβ and Gγ from the co-transfections with Gαi3-YFP and KB-1753-Nluc. Indeed, the responses to $\alpha2_A$-AR (Figures 1B and 1C) or MOR (Figures S1A and S1B) stimulation were the same in cells with or without Gβ/Gγ co-transfection. This suggests that exogenously expressed Gαi3-YFP associates with endogenous Gβγ subunits to yield functional Gαβγ trimers that are activated by GPCRs and that overexpression of Gβ and Gγ can be omitted. We also found that co-expression of the Gαi chaperone Ric-8A increased Gαi3-YFP expression and associated BRET responses, but this effect was too marginal to warrant its

Please cite this article in press as: Maziarz et al., Revealing the Activity of Trimeric G-proteins in Live Cells with a Versatile Biosensor Design, Cell (2020), https://doi.org/10.1016/j.cell.2020.06.020

CellPress

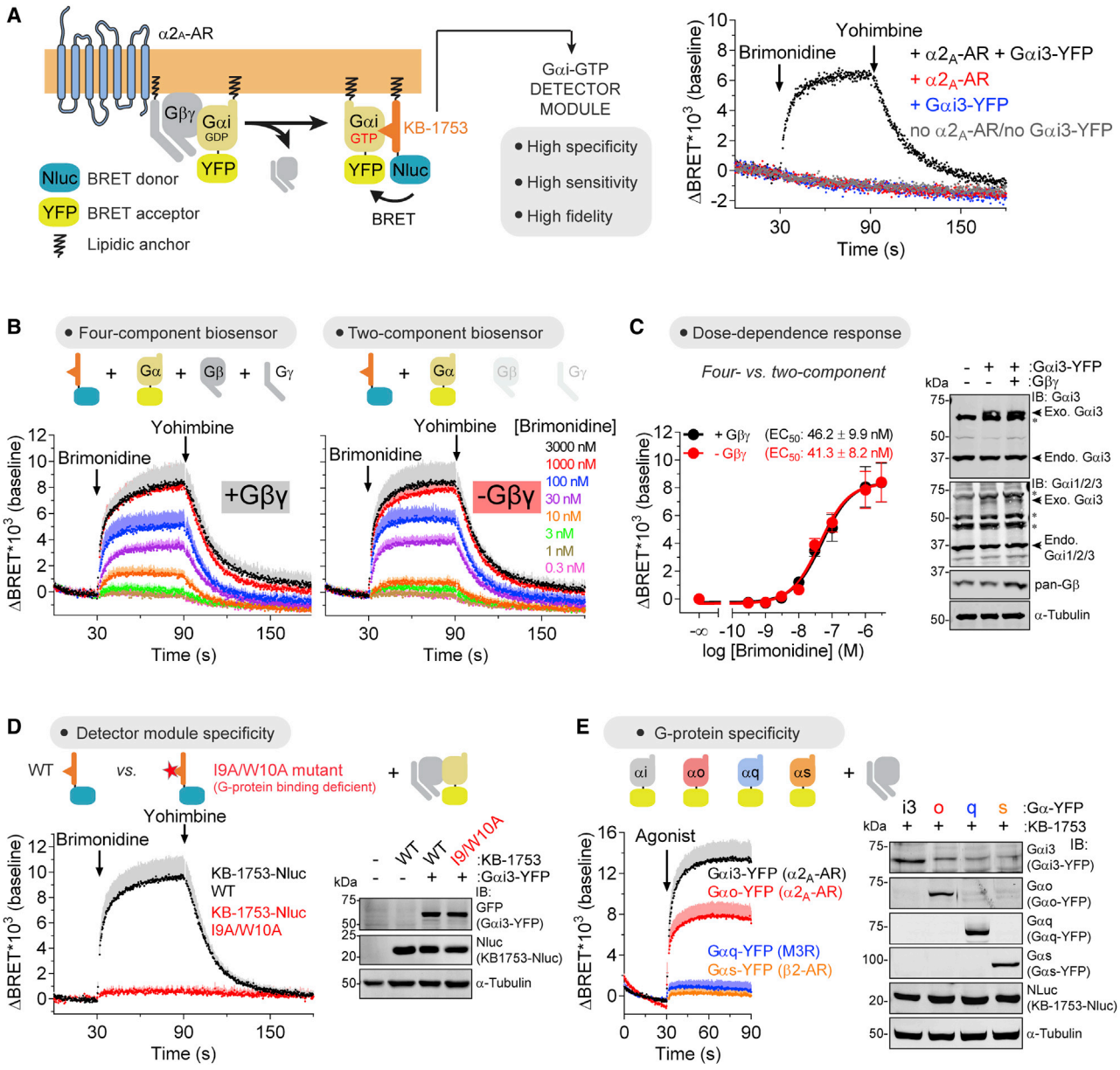

Figure 1. Direct Detection of GTP-Bound Gαi in Cells

(A) Gαi-GTP biosensor design principle and representative traces of BRET measurements in HEK293T cells expressing KB-1753-Nluc along with the indicated constructs. Brimonidine, 0.1 μM; yohimbine, 100 μM.

(B and C) Agonist dose-dependent Gαi-GTP responses using four- or two-component biosensors in HEK293T cells expressing $\alpha2_A$-AR. Time traces are shown in (B) and a semilogarithmic dose-dependence graph in (C). Mean ± SEM, n = 4. In (B), SEM is displayed as bars of lighter color than data points and only in the positive direction for clarity. Exo, exogenous; Endo, endogenous; *, non-specific immunoreactive band.

(D) Loss of Gαi-GTP response upon mutation of KB-1753-Nluc. Brimonidine, 1 μM; yohimbine, 100 μM. Mean ± SEM, n = 3–6.

(E) Detection of Gαi-GTP and Gαo-GTP but not Gαq-GTP or Gαs-GTP responses by KB-1753-Nluc upon GPCR agonist stimulation. Cells expressing G-proteins with the indicated cognate GPCRs were agonist stimulated as follows: Gαi3/Gαo, 5 μM brimonidine; Gαq, 100 μM carbachol; Gαs, 100 μM isoproterenol. Mean ± SEM, n = 4.

See also Figure S1.

inclusion as an additional genetic component of the biosensor system (Figure S1D).

We confirmed the specificity of the biosensor by showing that a KB-1753 mutation known to disrupt G-protein binding (Johnston et al., 2006) also prevented an agonist-induced BRET increase upon GPCR stimulation (Figure 1D; Figure S1C). Moreover, BRET responses were observed in cells expressing Gα subunits of the $G_{i/o}$ family (Gαi3-YFP and Gαo-YFP) but not of

Please cite this article in press as: Maziarz et al., Revealing the Activity of Trimeric G-proteins in Live Cells with a Versatile Biosensor Design, Cell (2020), https://doi.org/10.1016/j.cell.2020.06.020

other families, such as Gαq-YFP or Gαs-YFP, upon stimulation of their cognate GPCRs (Figure 1E), despite confirmation of robust Gq or Gs activation using a free Gβγ biosensor that is agnostic to the Gα subtype (Hollins et al., 2009; Masuho et al., 2015; Figure S1E). Overall, these controls rule out that BRET responses observed with the Gαi3-YFP/KB-1753 pair are due to non-specific interactions between these membrane-associated components, indicating instead that the BRET responses reflect specific interactions between the KB-1753 detector module and its target G-protein.

The Gαi-GTP Biosensor Directly Monitors the GDI Activity of GoLoco Motifs

As a proof of principle for the utility of the Gαi-GTP biosensor to capture features of G-protein regulation not captured by Gα-Gβγ dissociation biosensors, we implemented it to study the function of GoLoco motifs. These are protein sequences that confer GDI activity toward Gαi proteins *in vitro*; i.e., they block formation of Gαi-GTP by precluding nucleotide exchange (Sato et al., 2006; Willard et al., 2004). However, GoLoco motifs also cause dissociation of Gβγ from Gαi in the absence of nucleotide exchange (Ghosh et al., 2003; Webb et al., 2005). To date, it has not been possible to directly determine whether GoLoco motifs work as GDIs in cells to preclude Gαi-GTP formation. To address this point, we used a previously described (Parag-Sharma et al., 2016) synthetic biology approach to control the activity of the GoLoco motif of RGS12 (R12-GoLoco) (Kimple et al., 2002) in HEK293T cells expressing Gαi-GTP or free Gβγ biosensors (Figure 2A). Essentially, we used rapamycin-induced dimerization to "activate" R12-GoLoco by recruiting it from the cytosol to membranes, bringing the G-protein regulator into close proximity to its membrane-bound substrate Gαi (Parag-Sharma et al., 2016; Figure 2A). Consistent with the previously reported ability of GoLoco motifs to dissociate Gα-Gβγ *in vitro* (Ghosh et al., 2003; Webb et al., 2005) and promote Gβγ-dependent signaling in yeast (Cismowski et al., 1999), rapamycin caused a rapid BRET increase in cells expressing the free Gβγ biosensor (Figure 2B). In contrast, no change in BRET was observed upon rapamycin stimulation of cells expressing the Gαi-GTP biosensor (Figure 2B). Together, these findings indicate that R12-GoLoco can promote release of Gβγ in the absence of nucleotide exchange. Next we investigated the effects of R12-GoLoco under conditions of active nucleotide exchange (Figure 2C). Although R12-GoLoco is a GDI *in vitro* and would be expected to dampen GPCR-initiated G-protein activity, we found that addition of rapamycin after GPCR stimulation further enhanced the BRET response in cells expressing the free Gβγ biosensor (Figure 2C). This can be explained by the ability of GoLoco motifs to further promote Gα-Gβγ dissociation independent of nucleotide exchange (Figure 2B). Only in cells expressing the Gαi-GTP biosensor did we capture the inhibition of GPCR-mediated activation that would be expected from a GDI (Figure 2C), providing direct evidence in cells for the GDI activity of GoLoco motifs previously characterized biochemically *in vitro*. These results indicate that Gαi-GTP biosensors can capture modes of G-protein regulation in cells that cannot be captured by biosensors that detect Gα-Gβγ dissociation, such as the GDI activity of GoLoco motifs.

Rational Design of Unimolecular G-protein Activity Biosensors

The bi-molecular BRET system described above to detect Gαi-GTP still relies on exogenously expressed G-proteins. Our next goal was to develop a biosensor that could detect the activity of endogenously expressed G-proteins, for which we envisioned the design of unimolecular biosensors. This design is based on the unique properties of the so-called "ER/K α helices" (Sivaramakrishnan and Spudich, 2011), which tend to exist in a fully extended conformation that spans tens of nanometers but also display low-frequency stochastic bending that brings the two ends of the helix into close proximity (Figure 3A). The ratio of "bent" versus "open" conformation species can be increased by external constraints, like the interaction between two protein domains attached to the ends of the ER/K helix (Sivaramakrishnan and Spudich, 2011; Swanson and Sivaramakrishnan, 2014). We reasoned that this could be exploited to make unimolecular G-protein activity BRET biosensors based on two principles of design by modules. First, the ER/K α helix (~10 nm) would function as a linker between the BRET donor and acceptor modules (Nluc and YFP, respectively) to minimize BRET under resting conditions (Figure 3A). Second, a membrane-anchoring sequence and an active G-protein detector module (e.g., KB-1753) would be fused at opposite ends of the biosensor. Because G-protein activation occurs on cell membranes, we reasoned that this design would favor the bent conformation of the ER/K linker when the detector module binds to active G-protein species on membranes (Figure 3A). In turn, the bent conformation of the ER/K linker would bring the BRET donor and acceptor modules into closer proximity, resulting in increased BRET (Figure 3A). We named this design "BERKY" (BRET biosensor with ER/K linker and YFP).

Validation of a Unimolecular Biosensor that Detects Endogenous Gαi-GTP

We first assessed the properties of a BERKY biosensor for Gαi-GTP (Gαi*-BERKY) constructed with the previously validated detector module KB-1753 (Figure 1). For this, we co-expressed the biosensor with the Gi3 wild type (WT), which is GDP bound under resting conditions, or the Gi3 Q204L mutant (QL), which is GTPase deficient and constitutively bound to GTP (Figure 3B). We also compared constructs with one, two, or three YFPs (Gαi*-BERKY1, Gαi*-BERKY2, and Gαi*-BERKY3, respectively) to investigate whether increasing the acceptor-to-donor ratio per biosensor molecule could improve the dynamic range and performance. We found that BRET was higher in HEK293T cells expressing Gi3 QL compared with cells expressing Gi3 WT and that the difference in amplitude was proportional to the number of acceptor modules (YFP) in BERKY (Figure 3B). Next we carried out kinetic BRET measurements with cells expressing exogenous Gi3 WT or only endogenous G-proteins. We found that $\alpha 2_A$-AR (Figure 3C) or MOR (Figure S2A) stimulation led to a rapid increase in BRET that was reversed upon addition of an antagonist in cells expressing exogenous Gi3 and in cells expressing only endogenous G-proteins, but with larger amplitude for the former compared with the latter. Consistent with the steady-state measurements using Gi3 QL (Figure 3B), the amplitude of

Please cite this article in press as: Maziarz et al., Revealing the Activity of Trimeric G-proteins in Live Cells with a Versatile Biosensor Design, Cell (2020), https://doi.org/10.1016/j.cell.2020.06.020

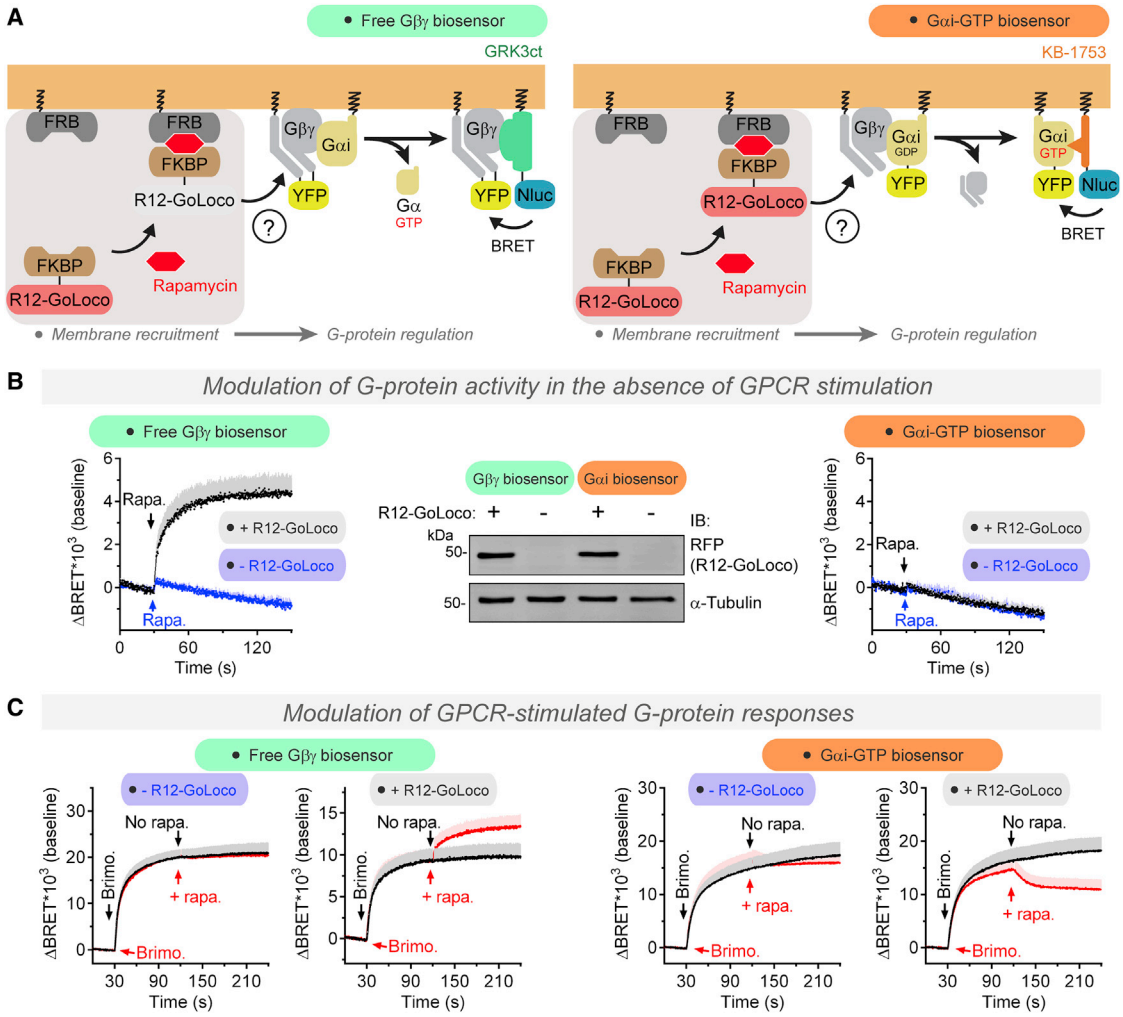

Figure 2. Differential Regulation of Free Gβγ and Gαi-GTP Levels by GoLoco Motifs

(A) Real-time measurement of free Gβγ or Gαi-GTP levels in cells upon rapamycin-induced rapid recruitment of the R12-GoLoco GDI to cell membranes.

(B) Membrane recruitment of R12-GoLoco promotes Gβγ release from Gαi-Gβγ trimers but does not change basal levels of Gα-GTP in HEK293T cells. Mean ± SEM, n = 4. Rapa, rapamycin.

(C) Membrane recruitment of R12-GoLoco diminishes GPCR-stimulated ($\alpha2_A$-AR) levels of Gαi-GTP in cells, whereas it further promotes dissociation of Gαi-Gβγ trimers in HEK293T cells. Mean ± SEM, n = 3–5. Brimo, brimonidine (3 nM).

the $\alpha2_A$-AR-mediated responses was proportional to the number of BRET acceptor modules per biosensor (Figure 3C), indicating that Gαi*-BERKY3 had the most robust performance. Next we assessed the specificity of the observed response by using pertussis toxin (Ptx), which specifically ADP-ribosylates Gi proteins to prevent their coupling to GPCRs. We found that $\alpha2_A$-AR-stimulated BRET increases were completely blunted after pre-treatment with Ptx (Figure S2B) but not affected in cells expressing a Ptx-insensitive Gαi3 mutant (Figure S2C). These results indicate that Gαi*-BERKY3 can specifically measure activation of endogenous Gi proteins in cells.

We also attempted an alternative Gαi*-BERKY3 design by replacing the KB-1753 detector module with another related peptide, KB-1746, reported previously to also recognize Gα-GTP species of the $G_{i/o}$ family (Johnston et al., 2008). However, this alternative biosensor design failed to report any response in cells expressing $G_{i/o}$ proteins (Figure S2D).

Because it has not been possible in the past to directly measure the activation properties of endogenously expressed Gi, we carried out a detailed analysis of its activation kinetics using Gαi*-BERKY3 and compared it with the activation kinetics in cells expressing exogenous Gαi3/Gβγ upon stimulation of $\alpha2_A$-AR. Endogenous Gi activation data fit well to a one-component exponential association curve, from which we determined an activation half-time ($t_{1/2}$) of ~250 ms (Figure 3D). On the other hand, cells expressing exogenous Gi proteins displayed slower rates of activation, with a $t_{1/2}$ of ~1,300 ms, which is consistent with previously reported values using overexpressed, fluorescently tagged Gi proteins in FRET measurements with the same GPCR (Bünemann et al., 2003). Moreover, activation

Please cite this article in press as: Maziarz et al., Revealing the Activity of Trimeric G-proteins in Live Cells with a Versatile Biosensor Design, Cell (2020), https://doi.org/10.1016/j.cell.2020.06.020

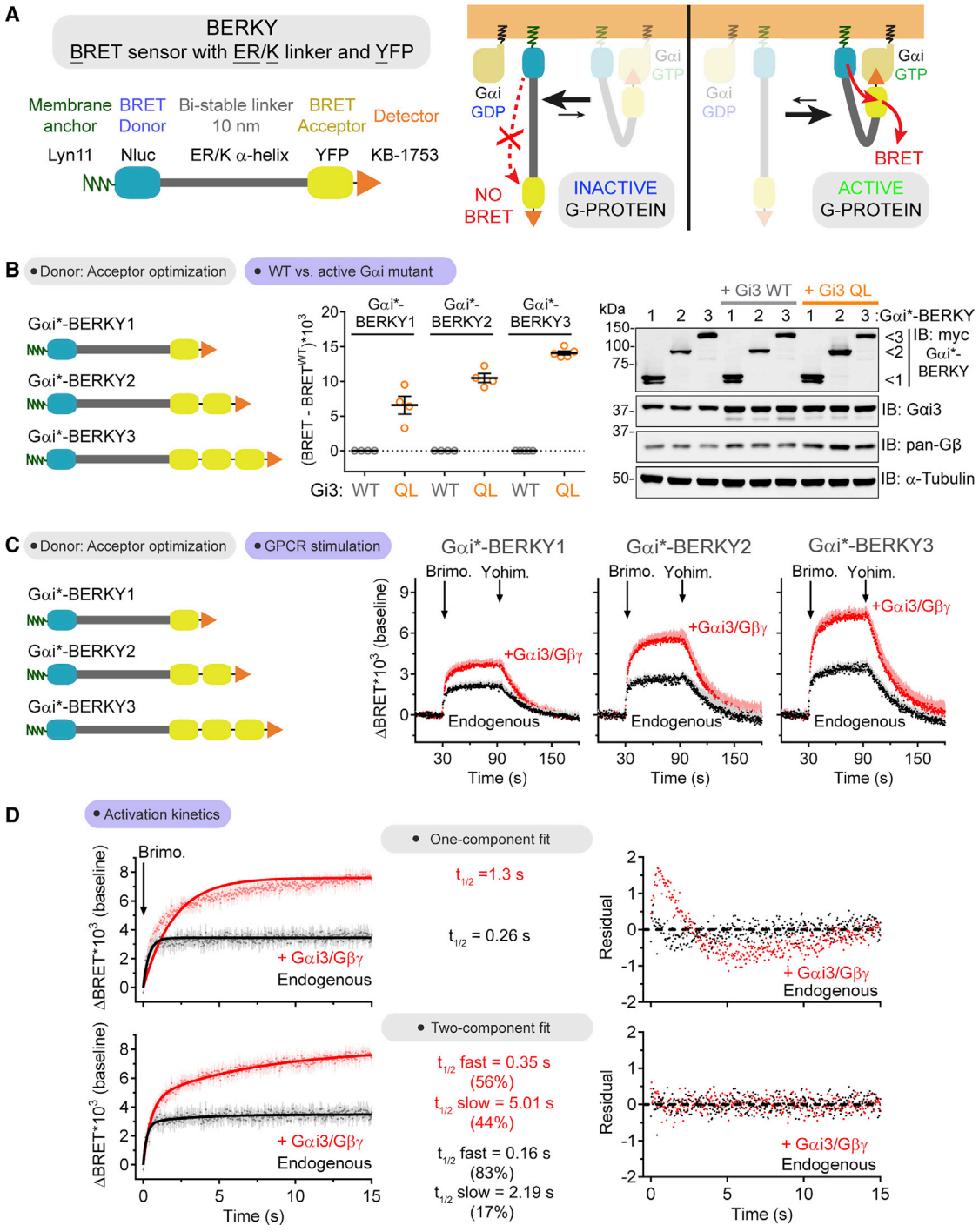

Figure 3. Detection of Endogenous Gαi-GTP in Cells with a Unimolecular Biosensor

(A) Modular design of a unimolecular biosensor for Gαi-GTP (Gαi*) and the rationale for BRET enhancement upon G-protein activation.

(B and C) Increasing the number of BRET acceptor modules (YFP) relative to donor modules (Nluc) per Gαi*-BERKY biosensor molecule enhances the BRET increases observed upon expression of a constitutively active G-protein mutant (Gi3 QL, B) or upon GPCR stimulation ($\alpha 2_A$-AR, C). Mean ± SEM, n = 3–5.

(D) Gαi activation kinetics were determined in HEK293T cells expressing Gαi*-BERKY3 with or without Gαi3/Gβγ overexpression upon GPCR stimulation ($\alpha 2_A$-AR, 5 μM Brimo). Data points are mean ± SEM (n = 4), and solid lines are fits to one-component exponential curves (top) or two-component exponential curves (bottom). Residual plots for each of the curve fits are shown on the right.

See also Figure S2.

data in cells expressing exogenous Gi proteins displayed significant deviations from the fit to a one-component exponential association curve (Figure 3D). Instead, these data fit better to a two-component exponential association curve (Figure 3D), which revealed a fast component with a $t_{1/2}$ similar to that measured for activation of endogenous G-proteins (i.e., ~350 ms) and a slow component with a $t_{1/2}$ in the range of several seconds. We ruled out that the slower activation kinetics in cells expressing exogenous Gi is due to excess Gβγ subunits that might dampen activation because we found that expression of Gβγ alone did not alter the activation kinetics compared with cells expressing only endogenous G-proteins (Figure S2E). Also, in G-protein dose dependence studies, we found slower activation kinetics even when low amounts of exogenous Gi3 were expressed (Figure S2F). We speculate that the fast component of the activation kinetics could represent a pool of G-proteins that is readily accessible and rapidly activated by GPCRs, whereas the slow component arises from activation of G-proteins that are only accessed when the GPCR progressively disengages from already activated G-proteins. This could explain why, for endogenous G-proteins, the two-component fit is only marginally better than the one-component fit and why the contribution of the slow component in the two-component fit is minimal (~15%) (Figure 3D), whereas, in the presence of additional exogenous G-proteins, the two-component fit is much better than the one-component fit, and the contribution of the slow component in the two-component fit is much more pronounced (~50%) (Figure 3D). Regardless of this speculation, our side-by-side comparison with the same biosensor (i.e., Gαi*-BERKY3) reveals that G-protein activation kinetics are distorted upon expression of exogenous G-proteins.

Direct and Specific Detection of Gαq-GTP and Gα13-GTP

Next we set out to develop additional probes to detect Gα-GTP species from families other than $G_{i/o}$ as a direct measure of activation of G-proteins. Analogous to the approach for Gαi-GTP, this was done in a bi-molecular BRET format with exogenously expressed G-proteins as a step that preceded the BERKY design with endogenously expressed G-proteins. First, we sought to identify a detector module for Gαq-GTP ($G_{q/11}$ family). Following the same specificity, sensitivity, and fidelity criteria as for Gαi (Figure 4A), we reasoned that the Regulator of G protein Signaling (RGS) homology (RH) domain of GRK2 ($GRK2^{RH}$) could serve as the detector module for GTP-bound Gαq because it binds specifically and with high affinity to active $G_{q/11}$ α subunits without perturbing their intrinsic ability to bind or hydrolyze nucleotides (Carman et al., 1999; Day et al., 2004; Sterne-Marr et al., 2003; Tesmer et al., 2005). Indeed, co-expression of internally tagged Gαq-YFP with $GRK2^{RH}$-Nluc resulted in a BRET biosensor with properties analogous to those of the Gαi-GTP biosensor. First, it reported rapid activation upon M3 muscarinic receptor (M3R) stimulation (Figures 4A and 4B). This BRET response was sustained for at least 15 min (Figure S3A) but could be rapidly reversed to baseline upon addition of a GPCR antagonist (Figures 4A and 4B). The Gαq-GTP response was also agonist dose dependent (Figures 4B and 4C), did not require co-expression of Gβ/Gγ for robust performance (Figures 4B and 4C), and could be reproduced by stimulation of a second Gq-coupled GPCR ($\alpha 1_A$-AR; Figure S3B). Specificity was further supported by loss of response upon introduction of a GRK2 mutation reported previously to prevent Gαq binding (Day et al., 2004; Figure 4D) and by lack of response upon GPCR-mediated activation of Gαs, Gαi3, or Gαo (Figure 4E).

We also confirmed robust, dose-dependent, reversible, and specific detection of Gα13-GTP ($G_{12/13}$ family) with or without co-transfection of Gβ and Gγ (Figure S4) by using an analogous bi-molecular BRET biosensor that leverages as a detector module the RH domain of PDZ-RhoGEF (PRG^{RH}), which binds specifically to Gα13-GTP with high affinity but without affecting G-protein enzymatic activity (Chen et al., 2008; Wells et al., 2002).

Taken together, these findings show that Gα-GTP formed from three different G-protein families ($G_{i/o}$, $G_{q/11}$, and $G_{12/13}$) can be specifically detected with sensitivity and fidelity using a biosensor design of only two genetic components: Gα internally tagged with a YFP and a Gα-GTP detector module fused to Nluc.

The Gαq-GTP Biosensor Reveals the Properties of Cancer-Associated Mutations at Gαq R247

To further showcase the utility of Gα-GTP probes for direct detection of G-protein activity, we implemented the Gαq-GTP biosensor to characterize cancer-associated Gαq mutants (Figure 5A). We used previously characterized cancer mutations of Q209 and R183 to benchmark the biosensor and picked uncharacterized mutations of R247 for further investigation. Although R247 mutations are not as frequent as Q209 or R183 mutations (Cerami et al., 2012), which cause a large fraction of uveal melanomas (Chua et al., 2017) and Sturge-Weber syndrome (Shirley et al., 2013), this amino acid is in a position near the nucleotide binding pocket fully conserved across all mammalian Gα proteins (Figure 5A), and genetic evidence in *C. elegans* suggests that its mutation might yield a gain-of-function (*egl-30(tg26)*) genotype (Doi and Iwasaki, 2002). As expected, mutants Q209L and R183C exhibited high levels of BRET under unstimulated conditions and failed to elicit significant increases upon maximal stimulation of the GPCR M3R in HEK293T cells (Figures 5B and 5C), which is consistent with their previously reported constitutive activity because of deficient GTPase activity. Also in agreement with previous characterizations, the constitutive activity of R183C, but not of Q209L, was partially suppressed by RGS8, a GAP for Gαq, in unstimulated cells (Berman et al., 1996). For the R247Q and R247L mutants, we found that, although basal BRET was not increased and they invoked BRET responses similar to the WT, their GPCR-mediated response was not affected by RGS8, whereas it was decreased ~50% for the WT (Figure 5B). These results suggest that R247 mutants might be insensitive to the GAP activity of RGS proteins despite not having high constitutive activity. We leveraged the kinetic resolution and sensitivity of the Gαq-GTP biosensor to further investigate this point, resulting in two observations that were consistent with GAP insensitivity. First, the rate of deactivation upon addition of a GPCR antagonist was slower for R247 mutants (Figure 5D), and second, there was a leftward shift of the agonist dose dependence curve (Figure 5E) compared with the WT. Because these features closely resemble observations of a previously described synthetic mutant that specifically precludes RGS

Please cite this article in press as: Maziarz et al., Revealing the Activity of Trimeric G-proteins in Live Cells with a Versatile Biosensor Design, Cell (2020), https://doi.org/10.1016/j.cell.2020.06.020

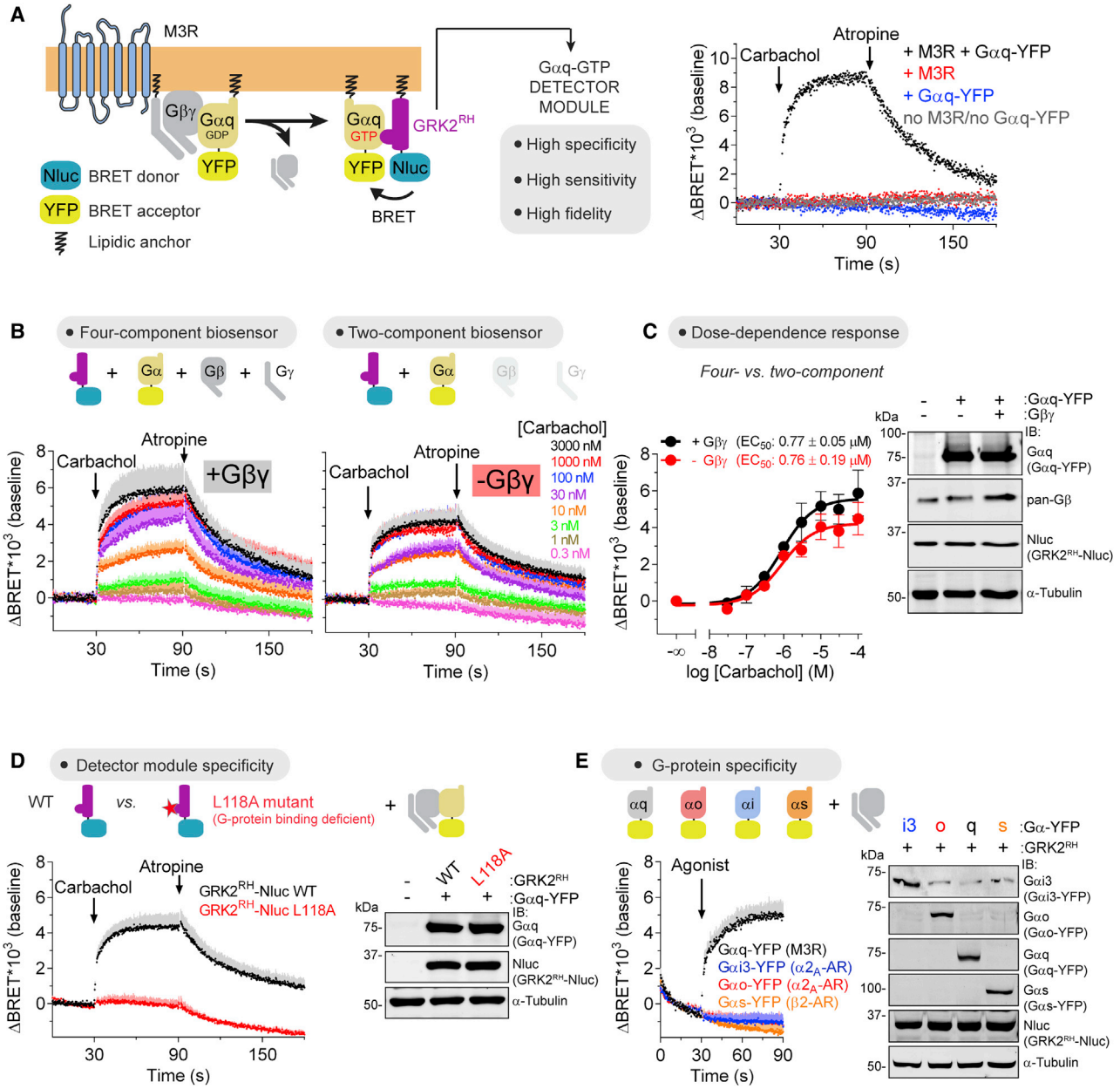

Figure 4. Direct Detection of GTP-Bound Gαq in Cells

(A) Gαq-GTP biosensor design principle and representative traces of BRET measurements in HEK293T cells expressing GRK2^{RH}-Nluc along with the indicated constructs. Carbachol, 100 μM; atropine, 100 μM.

(B and C) Agonist dose-dependent Gαq-GTP responses using four- or two-component biosensors in HEK293T cells expressing M3R. Time traces are shown in (B) and a semilogarithmic dose-dependence graph in (C). Mean ± SEM, n = 4–6.

(D) Loss of Gαq-GTP response upon mutation of GRK2^{RH}-Nluc. Carbachol, 30 μM; atropine, 100 μM. Mean ± SEM, n = 3–7.

(E) Detection of Gαq-GTP but not Gαi3-GTP, Gαo-GTP, or Gαs-GTP responses by GRK2^{RH}-Nluc upon GPCR agonist stimulation. Cells expressing G-proteins with the indicated cognate GPCRs were agonist stimulated as follows: Gαq, 100 μM carbachol; Gαi3/Gαo, 5 μM Brimo; Gαs, 100 μM isoproterenol. Mean ± SEM, n = 3–5.

See also Figures S3 and S4.

binding to G-proteins (Lambert et al., 2010; Lan et al., 1998), we tested whether R247 mutants also have impaired RGS binding and found that they do not bind to the RGS protein GAIP (Figure 5F). Although the precise effect of Gαq R247 mutants in cancer progression remains to be elucidated, our findings suggest that they have a gain of function because of a mechanism different from any other characterized Gαq oncogenic mutant. Instead of favoring activation by blunting the intrinsic GTPase

Please cite this article in press as: Maziarz et al., Revealing the Activity of Trimeric G-proteins in Live Cells with a Versatile Biosensor Design, Cell (2020), https://doi.org/10.1016/j.cell.2020.06.020

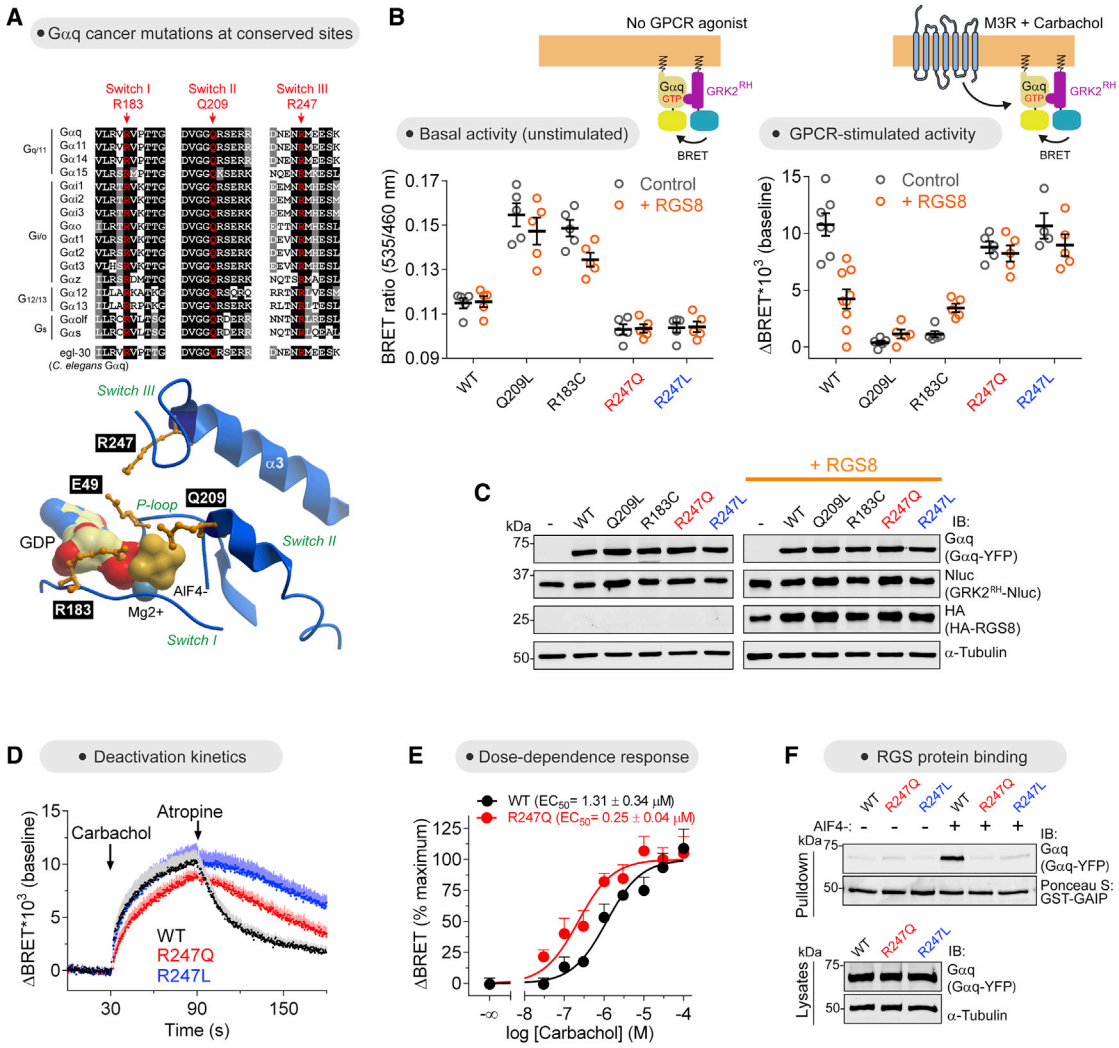

Figure 5. Characterization of Cancer-Associated G-protein Mutants with a Gαq-GTP Biosensor

(A) Alignment of Gα switch regions, showing in red three fully conserved positions that are mutated in Gαq in cancer. A three-dimensional model of Gαq (PDB: 3OHM) shows the position of selected residues around the nucleotide binding site.

(B) Different activation properties of cancer-associated Gαq mutants as determined by the Gαq-GTP biosensor GRK2^{RH}-Nluc. Gαq-GTP levels were determined with and without GPCR stimulation (M3R; carbachol, 100 μM) and in the absence (gray) or presence (orange) of the GAP RGS8. Mean ± SEM, n = 4–9.

(C) Representative immunoblot of cells used for the experiment shown in (B).

(D) R247 mutants deactivate more slowly than Gαq WT upon termination of GPCR stimulation, as determined by the Gαq-GTP biosensor GRK2^{RH}-Nluc. Mean ±, n = 4–5. Carbachol, 100 μM; atropine, 100 μM.

(E) Carbachol activates Gαq R247Q 5-fold more potently than Gαq WT, as determined by the Gαq-GTP biosensor GRK2^{RH}-Nluc. Mean ± SEM, n = 4.

(F) Gαq R247 mutants do not bind to the RGS protein GAIP. Binding to immobilized GST-GAIP was determined in the absence or presence of AlF_4^-, which induces the G-protein activation transition-state conformation recognized by RGS proteins. Shown is one experiment of n > 3.

See also Figure S5.

activity of Gαq, the R247 mutations favor activation by rendering Gαq insensitive to the GAP activity of RGS proteins. Thus, the Gαq-GTP biosensor can be implemented to gain mechanistic insights into G-protein dysregulation in cancer.

The Gα13-GTP Biosensor Reveals Hyperactive G_{13} Mutants in Bladder Cancer

Next we pursued implementation of the Gα13-GTP biosensor to characterize other cancer mutations. Mining data in cBioportal (Cerami et al., 2012), we noticed that Gα13 is mutated in bladder cancer with moderate frequency (~2%) and that R200 appears to be a mutation hotspot (Figure S5A). R200 is in a position conserved across all mammalian Gα proteins, and its mutation in other Gα proteins renders them oncogenic because of hyperactivation (e.g., it is the same position as R183 in Gαq described above) (Landis et al., 1989; Lyons et al., 1990; Pace et al., 1991; Van Raamsdonk et al., 2009). We tested the hypothesis that R200 mutation in Gα13 also

Please cite this article in press as: Maziarz et al., Revealing the Activity of Trimeric G-proteins in Live Cells with a Versatile Biosensor Design, Cell (2020), https://doi.org/10.1016/j.cell.2020.06.020

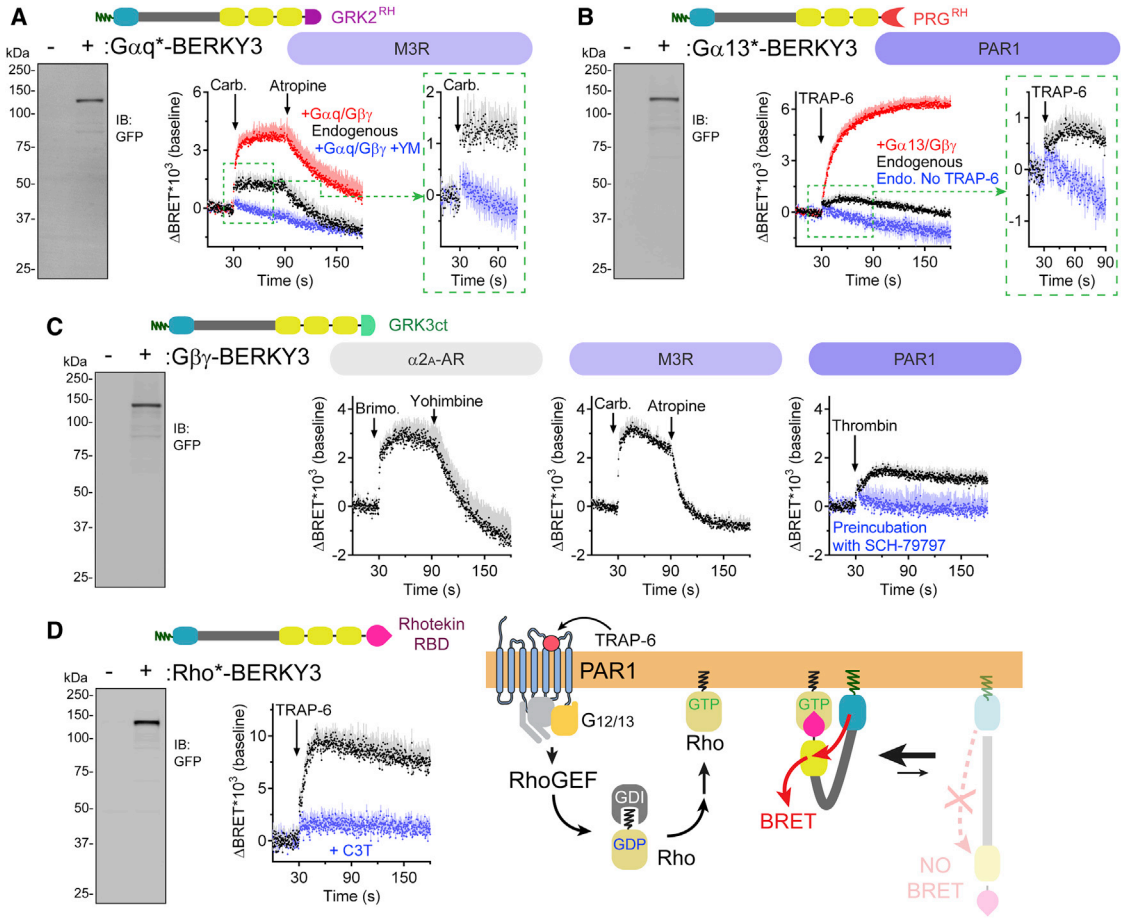

Figure 6. Detection of Endogenous Gαq-GTP, Gα13-GTP, Free Gβγ, and Rho-GTP in Cells with Unimolecular Biosensors

(A) BRET response detected with Gαq*-BERKY3 upon M3R modulation in HEK293T cells expressing exogenous Gαq/Gβγ or only endogenous G-proteins. BRET of cells expressing exogenous Gαq/Gβγ and pre-treated with 10 μM YM-254890 for 10 min is shown in blue. Carbachol, 100 μM; atropine, 100 μM. Mean ± SEM, n = 4.

(B) BRET response detected with Gα13*-BERKY3 upon PAR1 stimulation in HEK293T cells expressing exogenous Gα13/Gβγ or only endogenous G-proteins. BRET of unstimulated cells (blue) is shown for reference. TRAP-6, 30 μM. Mean ± SEM, n = 4–6.

(C) BRET responses detected with Gβγ-BERKY3 upon modulation of $\alpha 2_A$-AR, M3R, or PAR1, as indicated, in HEK293T cells expressing only endogenous G-proteins. Brimo, 5 μM; yohimbine, 25 μM; carbachol, 100 μM; atropine, 100 μM; thrombin, 1 U/mL; SCH-79797, 40 μM. Mean ± SEM, n = 3–4.

(D) BRET responses detected with Rho*-BERKY3 upon PAR1 stimulation in HEK293T cells co-transfected (blue) or not (black) with the Rho inhibitor C3 toxin (C3T). TRAP-6, 30 μM. Mean ± SEM, n = 4.

results in G-protein hyperactivation by using our Gα13-GTP biosensor. We found that R200G and R200K cancer mutants caused a marked increase in BRET similar to that observed for an artificial GTPase-deficient mutant (Q226L) that causes G-protein hyperactivation and oncogenic transformation (Voyno-Yasenetskaya et al., 1994; Xu et al., 1994) and that stimulation of a cognate GPCR did not enhance BRET for any of the mutants (Figures S5B and S5C), indicating that they are constitutively active. We confirmed that R200 mutants lead to enhanced activation of downstream signaling targets by using a transcriptional reporter known to be activated by a $G_{12/13}$-dependent pathway (O'Hayre et al., 2016; Figure S5D). These findings suggest that Gα13 R200 mutants are hyperactive, showcasing the power of the Gα13-GTP biosensor to reveal signaling functions of cancer-associated mutants.

Modular Design of Unimolecular Biosensors for Different Active G Protein Species

Because the unimolecular BERKY biosensor relies on a modular design (Figure 3), we asked whether replacing the detector module specific for Gαi-GTP (i.e., KB-1753) would be sufficient to generate unimolecular biosensors for other G-protein active species. The resulting unimolecular biosensors could then be used to detect activation of different endogenous G-proteins. For this, we leveraged the previous characterization of other detector modules in bi-molecular BRET biosensors, like $GRK2^{RH}$ and PRG^{RH} (Figure 4; Figure S4). Replacing KB-1753 with $GRK2^{RH}$ resulted in the Gαq-GTP biosensor Gαq*-BERKY3 (Figure 6A), which reported a reversible increase in BRET upon M3R stimulation of HEK293T cells overexpressing exogenous Gαq or expressing only endogenous G-proteins. The $G_{q/11}$-specific

Please cite this article in press as: Maziarz et al., Revealing the Activity of Trimeric G-proteins in Live Cells with a Versatile Biosensor Design, Cell (2020), https://doi.org/10.1016/j.cell.2020.06.020

inhibitor YM-254890 completely blunted the response, confirming specificity. Similarly, implementation of PRG^{RH} as the detector module resulted in Gα13*-BERKY3 (Figure 6B), which reported a BRET increase upon stimulation of PAR1 in HEK293T cells overexpressing exogenous Gα13 or, to a lesser extent, in cells expressing only endogenous G-proteins. Taken together, these results indicate that the unimolecular BERKY biosensor design can be adapted to detect endogenous Gα-GTP species from three different G-protein families ($G_{i/o}$, $G_{q/11}$, and $G_{12/13}$).

We reasoned that a similar approach could also be implemented to create a unimolecular BERKY biosensor for free Gβγ, allowing detection of another active signaling species of endogenously expressed trimeric G-proteins. For this, we used the C-terminal region of GRK3 (GRK3ct) as the detector module to generate Gβγ-BERKY3 (Figure 6C). This biosensor worked as expected because we observed a reversible increase in BRET upon $\alpha2_A$-AR stimulation of HEK293T cells expressing only endogenous G-proteins (Figure 6C). Because free Gβγ subunits are, in principle, formed upon activation of any G-protein, we reasoned that Gβγ-BERKY3 might detect activation downstream of diverse GPCRs, including those that do not couple preferentially to $G_{i/o}$. Consistent with this idea, we detected a BRET increase in cells expressing Gβγ-BERKY3 (and no exogenous G protein) in response to stimulation of the GPCRs M3R and PAR1 (Figure 6C). We also found that formation of free Gβγ occurred at a rate indistinguishable from that of Gαi-GTP formation ($t_{1/2}$, ~200 ms), as determined by Gβγ-BERKY3 and Gαi*-BERKY3, respectively (Figure S2G). These results provide direct evidence that nucleotide exchange and Gα-Gβγ dissociation occur simultaneously, at least within the subsecond resolution of our assay, upon GPCR-catalyzed activation of endogenous G-proteins.

Finally, we expanded our BERKY design implementation to another class of G-proteins: Rho GTPases. For this, we used the RBD domain of Rhotekin as the detector module for Rho-GTP (Figure 6D). We found that activation of the GPCR PAR1, which is known to activate a $G_{12/13}$-RhoA signaling axis (O'Hayre et al., 2016), led to increased BRET in cells expressing the Rho*-BERKY3 biosensor (Figure 6D). This response was abrogated by co-expressing the C3 toxin of *Clostridium botulinum* (C3T), a well-characterized inhibitor of Rho GTPases, demonstrating that Rho*-BERKY3 specifically detects activation of endogenous Rho GTPases.

Detection of G Protein Activity under Fully Native Conditions in Cells

The evidence presented so far shows that BERKY biosensors can detect activation of endogenously expressed G-proteins in the presence of exogenous GPCRs. To test whether BERKY biosensors can detect activation of endogenous G-proteins by endogenous GPCRs, we turned to HeLa cells, which express endogenous α2-ARs (Gibson and Gilman, 2006). Transient transfection of Gαi*-BERKY3 in HeLa cells yielded measurable, reversible BRET responses upon α2-AR stimulation (Figure S6A), so we generated HeLa cell lines stably expressing Gαi*-BERKY3 or Gβγ-BERKY3 by lentiviral transduction for increased reproducibility (Figure 7A; Figures S6B and S6C). We found that stimulation of these cells with an α2-AR agonist led to a dose-dependent (EC_{50}, ~10 nM) rapid increase in BRET (Figures 7B and 7C). Gαi-GTP- and Gβγ-dependent responses were reverted by an α2-AR antagonist and completely blunted by Ptx (Figures 7B and 7C), confirming the expected specificity of the biosensors. Using a different cell line, SH-SY5Y, we found that Gαi*-BERKY3 and Gβγ-BERKY3 can also detect activation of endogenous G-proteins upon stimulation of two different GPCRs endogenously expressed in these cells (Levitt et al., 2011): the MOR and the delta opioid receptor (DOR; Figures S7A–S7C). Similarly, Gq-specific activation could be detected by Gαq*-BERKY3 upon stimulation of muscarinic receptors endogenously expressed in SH-SY5Y cells (Figures S7A and S7D). Taken together, these findings demonstrate that BERKY family biosensors can detect multiple endogenous G-protein active species in different cell types and in response to different endogenous GPCRs.

An inherent property of any biosensor is that it interacts with the target species it detects, raising the question of whether it interferes with the normal function of the target. As a proof of principle to address this possibility, we assessed whether Gαi*-BERKY3 or Gβγ-BERKY3 interferes with Gi-dependent signaling in HeLa cells upon α2-AR stimulation. We measured cyclic AMP (cAMP) and phospho-ERK1/2 (pERK), which have been shown previously to be controlled by Gαi-GTP and free Gβγ, respectively, upon activation of α2-AR (Koch et al., 1994; Leyme et al., 2017). Using the same HeLa cell lines as those used to detect G-protein activity by BRET (Figures 7A–7C), we found that neither Gαi*-BERKY3 nor Gβγ-BERKY3 alters α2-AR-mediated cAMP inhibition (Figure 7D) or pERK1/2 activation (Figure 7E) responses. This indicates that expression of Gαi*-BERKY3 or Gβγ-BERKY3 at levels that permit detection of the activity of endogenous G-proteins does not significantly interfere with G-protein signaling in cells.

Given the ability of Gαi*-BERKY3 and Gβγ-BERKY3 to detect the activity of endogenous G-proteins in cell lines, we set out to determine whether they would also be powerful enough to detect it in a more physiologically relevant system. We chose primary cultures of cortical neurons because they recapitulate many of the cell-autonomous physiological responses of neurons, including the GPCR/G-protein signaling machinery responsible for slow (metabotropic) neuromodulation. We acutely transduced cortical neurons with lentiviruses for expression of Gαi*-BERKY3, Gβγ-BERKY1, or Gαq*-BERKY1 under a neuron-specific promoter (human Synapsin [hSyn]) and measured BRET upon GPCR modulation (Figure 7F). Stimulation of α2-AR (brimonidine) or $GABA_B$ receptors (baclofen) elicited a rapid increase in BRET in neurons expressing Gαi*-BERKY3 or Gβγ-BERKY1 (Figures 7G and 7H), which reverted upon addition of an antagonist for each respective GPCR. These responses were blunted by Ptx (Figures 7G and 7H), confirming that the measured BRET responses report activation of endogenous Gi proteins. Similar observations were made with other variants of the Gαi-GTP biosensor (Figure S7E) or upon modulation of adenosine receptors in neurons expressing Gβγ-BERKY1 (Figure S7F). We also observed responses to agonists for muscarinic (carbachol) or class I glutamate metabotropic receptors ((S)-3,5-DHPG) in neurons expressing Gαq*-BERKY1 (Figure 7I), which were blunted by the $G_{q/11}$ inhibitor

Please cite this article in press as: Maziarz et al., Revealing the Activity of Trimeric G-proteins in Live Cells with a Versatile Biosensor Design, Cell (2020), https://doi.org/10.1016/j.cell.2020.06.020

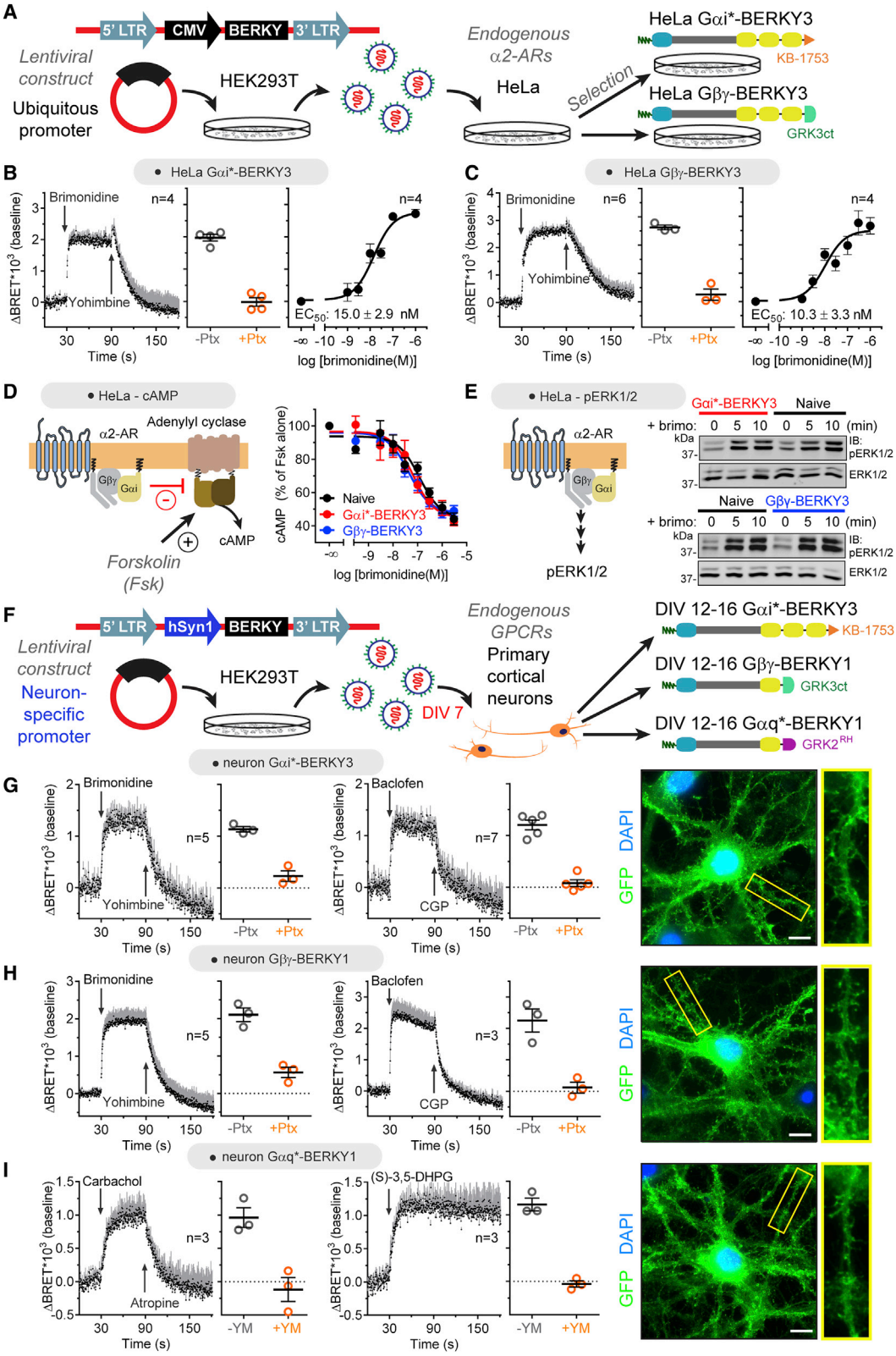

(legend on next page)

Please cite this article in press as: Maziarz et al., Revealing the Activity of Trimeric G-proteins in Live Cells with a Versatile Biosensor Design, Cell (2020), https://doi.org/10.1016/j.cell.2020.06.020

YM-254890. Taken together, these results show that BERKY biosensors can specifically detect activation of endogenous G-proteins in neurons in response to activation of many different types of neurotransmitter receptors.

Conclusions and Future Perspectives

The G-protein activity biosensors described here have numerous capabilities and features not afforded by other biosensors. An important capability is detection of activation of endogenous G-proteins, even upon stimulation of endogenous GPCRs, without measurable disturbance of normal G-protein signaling. Moreover, we presented biosensors that are unimolecular, which facilitates their implementation because only one genetic component has to be introduced into cells. This is showcased here by their implementation in four different cell types, including primary cultured neurons, which are typically considered poorly tractable for genetic manipulation. Furthermore, the unimolecular and bimolecular Gα biosensors developed here can directly detect Gα-GTP, which is highly complementary to currently used biosensors that can only monitor Gα-Gβγ dissociation. This idea is supported by our proof-of-principle experiments showing the utility of Gα-GTP biosensors to dissect mechanisms of G-protein modulation by regulators or by disease-associated mutations. Finally, the modular design of the biosensors described here makes them well suited for customization, adaptation, and/or optimization. Overall, the capabilities afforded by our suite of biosensors could be leveraged for GPCR drug development by allowing study of G-protein activation in greater depth and in more physiologically relevant systems.

Nevertheless, some limitations of these biosensors' design should be kept in mind. For example, there is room for improvement in the dynamic range of the BERKY unimolecular biosensors compared with their bi-molecular biosensor counterparts. However, the BERKY biosensor design presented here was not subjected to thorough optimization, which could include exploring different dipole orientations of the BRET donor and acceptor, implementing longer ER/K α helices (Sivaramakrishnan and Spudich, 2011), or modifying the flexible linkers between individual modules. Although the modularity of the biosensor design is a positive feature that allowed us to develop a suite of related probes, identifying the right detector modules can prove challenging. For example, we found that a Gα13-GTP biosensor based on the RH domain of p115-RhoGEF was less robust than the one based on PRG^{RH} (Figure S4B), and we have yet to identify a detector module for Gαs-GTP. Finally, the biosensors described here have good temporal resolution (sub-second) but no spatial resolution. A reasonable future goal is to convert these BRET biosensors into imaging-compatible probes based on FRET, which should be greatly facilitated by the modular nature of the BERKY design.

Although our BERKY biosensors can detect activation of endogenously expressed G-proteins, one potential concern is whether this reflects their true endogenous activity not modified by the presence of the biosensor. Expression of the biosensors at high levels could alter normal G-protein signaling because the detector modules utilized occlude the effector binding sites on their cognate G-protein targets. Although this is a general unavoidable caveat for virtually any biosensor, we provide direct evidence that expression of BERKY biosensors at low levels, but sufficient to allow robust detection of endogenous responses, does not measurably interference with downstream signaling (Figures 7A–7F).

GPCRs not only signal by coupling to G-proteins but also to arrestins (Weis and Kobilka, 2018). However, current biosensors for arrestin activation require exogenous arrestin expression, and, barring exceptions (Lee et al., 2016; Nuber et al., 2016), they also rely on bulky tags. Complementing biosensors that detect the activity of endogenous G-proteins with biosensors for endogenous arrestins would be very useful to rigorously probe the concept of ligand-induced biased signaling (Wisler et al., 2018).

In summary, here we presented a toolkit that allows investigation of G-protein activity in cells with unprecedented fidelity by using rational design principles that can be implemented to develop new or optimized biosensors.

STAR★METHODS

Detailed methods are provided in the online version of this paper and include the following:

Figure 7. Detection of Endogenous G-protein Activation by Endogenous GPCRs in Cell Lines and Primary Neurons

(A) Generation of HeLa cell lines stably expressing Gαi*-BERKY3 or Gβγ-BERKY3 to monitor G-protein activation upon activation of endogenously expressed α2-ARs.

(B and C) Endogenous Gαi-GTP (B) or free Gβγ (C) BRET responses detected by BERKY biosensors upon stimulation of endogenous α2-ARs in HeLa cells are reversible, pertussis toxin (Ptx) sensitive, and dose dependent. Unless otherwise indicated, Brimo was 5 μM and yohimbine 25 μM. Ptx, 0.2 μg/mL overnight. Mean ± SEM.

(D and E) Expression of Gαi*-BERKY3 or Gβγ-BERKY3 does not affect downstream Gi-dependent signaling upon stimulation of endogenous α2-ARs in HeLa cells. cAMP levels were determined upon stimulation with the indicated concentrations of Brimo in cells pretreated with 10 μM forskolin (D), and pERK1/2 levels were determined by immunoblotting upon stimulation with 3 μM Brimo (E).

(F) Acute lentiviral transduction of primary cortical neurons with Gαi*-BERKY3, Gβγ-BERKY1, or Gαq*-BERKY1 constructs to monitor G-protein activation upon stimulation of endogenously expressed GPCRs. DIV, days *in vitro*.

(G–I) Endogenous Gαi-GTP (G), free Gβγ (H), or Gαq-GTP (I) BRET responses detected by BERKY biosensors upon stimulation of endogenous GPCRs in primary cortical neurons. Responses to α2-AR (Brimo, 5 μM) or $GABA_BR$ (baclofen, 100 μM) are blocked by Ptx (0.2 μg/mL overnight preincubation), and responses to muscarinic receptors (carbachol, 100 μM) or class I metabotropic glutamate receptors ((S)-3,5-DHPG, 100 μM) are blocked by YM-254890 (YM, 10 μM, 10-min preincubation). Yohimbine, 25 μM; CGP 54626 (CGP), 1 μM (H) or 10 μM (G); atropine, 100 μM. Mean ± SEM. Wide-field fluorescence images of immunostained neurons show broad distribution of BERKY biosensors throughout the somata and dendrites. Scale bars, 10 μm.

See also Figure S7.

SUPPLEMENTAL INFORMATION

Supplemental Information can be found online at https://doi.org/10.1016/j.cell.2020.06.020.

ACKNOWLEDGMENTS

This work was supported by NIH grants R21MH118745, R01GM136132, and R01GM130120 (to M.G.-M.). M.M. was supported by American Cancer Society Funding Hope postdoctoral fellowship PF-19-084-01-CDD. We thank K. Martemyanov (Scripps Research Institute), N. Lambert (Augusta University), P. Wedegaertner (Thomas Jefferson University), J. Blumer and S. Lanier (Medical University of South Carolina), Mathew Layne (Boston University), and Richard Neubig (Michigan State University) for providing plasmids. We thank Vincent DiGiacomo for cloning the plasmid encoding Gα13-YFP and Lance Encell (Promega) for kindly providing the nanoluciferase antibody. We thank A. Amelio and K. Parag-Sharma (University of North Carolina, Chapel Hill) for providing the Lenti-X 293T cell line and related protocols of lentivirus production.

AUTHOR CONTRIBUTIONS

M.M., J.-C.P., A.L., A.M., A.G.-L., P.P.P., and M.G.-M. conducted the experiments. M.M., J.-C.P., A.L., and M.G.-M. designed the experiments. M.M., A.L., and M.G.-M. analyzed the data. M.M. and M.G.-M. wrote the manuscript. M.G.-M. conceived and supervised the project.

DECLARATION OF INTERESTS

M.G.-M. is listed as an inventor in a provisional patent filed by Boston University related to the content of this manuscript.

Received: February 14, 2020
Revised: April 21, 2020
Accepted: June 8, 2020
Published: July 6, 2020

REFERENCES

Berman, D.M., Wilkie, T.M., and Gilman, A.G. (1996). GAIP and RGS4 are GTPase-activating proteins for the Gi subfamily of G protein alpha subunits. Cell *86*, 445–452.

Bünemann, M., Frank, M., and Lohse, M.J. (2003). Gi protein activation in intact cells involves subunit rearrangement rather than dissociation. Proc. Natl. Acad. Sci. USA *100*, 16077–16082.

Carman, C.V., Parent, J.L., Day, P.W., Pronin, A.N., Sternweis, P.M., Wedegaertner, P.B., Gilman, A.G., Benovic, J.L., and Kozasa, T. (1999). Selective regulation of Galpha(q/11) by an RGS domain in the G protein-coupled receptor kinase, GRK2. J. Biol. Chem. *274*, 34483–34492.

Cerami, E., Gao, J., Dogrusoz, U., Gross, B.E., Sumer, S.O., Aksoy, B.A., Jacobsen, A., Byrne, C.J., Heuer, M.L., Larsson, E., et al. (2012). The cBio cancer genomics portal: an open platform for exploring multidimensional cancer genomics data. Cancer Discov. *2*, 401–404.

Chen, Z., Singer, W.D., Wells, C.D., Sprang, S.R., and Sternweis, P.C. (2003). Mapping the Galpha13 binding interface of the rgRGS domain of p115RhoGEF. J. Biol. Chem. *278*, 9912–9919.

Chen, Z., Singer, W.D., Danesh, S.M., Sternweis, P.C., and Sprang, S.R. (2008). Recognition of the activated states of Galpha13 by the rgRGS domain of PDZRhoGEF. Structure *16*, 1532–1543.

Chua, V., Lapadula, D., Randolph, C., Benovic, J.L., Wedegaertner, P.B., and Aplin, A.E. (2017). Dysregulated GPCR Signaling and Therapeutic Options in Uveal Melanoma. Mol. Cancer Res. *15*, 501–506.

Cismowski, M.J., Ma, C., Ribas, C., Xie, X., Spruyt, M., Lizano, J.S., Lanier, S.M., and Duzic, E. (2000). Activation of heterotrimeric G-protein signaling by a ras-related protein. Implications for signal integration. J. Biol. Chem. *275*, 23421–23424.

Cismowski, M.J., Takesono, A., Ma, C., Lizano, J.S., Xie, X., Fuernkranz, H., Lanier, S.M., and Duzic, E. (1999). Genetic screens in yeast to identify mammalian nonreceptor modulators of G-protein signaling. Nature Biotechnology *17*, 878–883.

Day, P.W., Tesmer, J.J., Sterne-Marr, R., Freeman, L.C., Benovic, J.L., and Wedegaertner, P.B. (2004). Characterization of the GRK2 binding site of Galphaq. J. Biol. Chem. *279*, 53643–53652.

De Vries, L., Mousli, M., Wurmser, A., and Farquhar, M.G. (1995). GAIP, a protein that specifically interacts with the trimeric G protein G alpha i3, is a member of a protein family with a highly conserved core domain. Proc. Natl. Acad. Sci. USA *92*, 11916–11920.

De Vries, L., Zheng, B., Fischer, T., Elenko, E., and Farquhar, M.G. (2000). The regulator of G protein signaling family. Annu. Rev. Pharmacol. Toxicol. *40*, 235–271.

DiGiacomo, V., Marivin, A., and Garcia-Marcos, M. (2018). When Heterotrimeric G Proteins Are Not Activated by G Protein-Coupled Receptors: Structural Insights and Evolutionary Conservation. Biochemistry *57*, 255–257.

Dohlman, H.G., and Thorner, J. (1997). RGS proteins and signaling by heterotrimeric G proteins. J. Biol. Chem. *272*, 3871–3874.

Doi, M., and Iwasaki, K. (2002). Regulation of retrograde signaling at neuromuscular junctions by the novel C2 domain protein AEX-1. Neuron *33*, 249–259.

Dorsam, R.T., and Gutkind, J.S. (2007). G-protein-coupled receptors and cancer. Nat. Rev. Cancer *7*, 79–94.

Druey, K.M., Blumer, K.J., Kang, V.H., and Kehrl, J.H. (1996). Inhibition of G-protein-mediated MAP kinase activation by a new mammalian gene family. Nature *379*, 742–746.

Farfel, Z., Bourne, H.R., and Iiri, T. (1999). The expanding spectrum of G protein diseases. N. Engl. J. Med. *340*, 1012–1020.

Galés, C., Van Durm, J.J., Schaak, S., Pontier, S., Percherancier, Y., Audet, M., Paris, H., and Bouvier, M. (2006). Probing the activation-promoted structural rearrangements in preassembled receptor-G protein complexes. Nat. Struct. Mol. Biol. *13*, 778–786.

Garcia-Marcos, M., Ghosh, P., and Farquhar, M.G. (2009). GIV is a nonreceptor GEF for G alpha i with a unique motif that regulates Akt signaling. Proc. Natl. Acad. Sci. USA *106*, 3178–3183.

Garcia-Marcos, M., Ghosh, P., Ear, J., and Farquhar, M.G. (2010). A structural determinant that renders G alpha(i) sensitive to activation by GIV/girdin is required to promote cell migration. J. Biol. Chem. *285*, 12765–12777.

Garcia-Marcos, M., Ghosh, P., and Farquhar, M.G. (2011). Molecular basis of a novel oncogenic mutation in GNAO1. Oncogene *30*, 2691–2696.

Garcia-Marcos, M., Ghosh, P., and Farquhar, M.G. (2015). GIV/Girdin transmits signals from multiple receptors by triggering trimeric G protein activation. J. Biol. Chem. *290*, 6697–6704.

Ghosh, M., Peterson, Y.K., Lanier, S.M., and Smrcka, A.V. (2003). Receptor- and nucleotide exchange-independent mechanisms for promoting G protein subunit dissociation. J. Biol. Chem. *278*, 34747–34750.

Ghosh, P., Garcia-Marcos, M., Bornheimer, S.J., and Farquhar, M.G. (2008). Activation of Galphai3 triggers cell migration via regulation of GIV. J. Cell Biol. *182*, 381–393.

Gibson, S.K., and Gilman, A.G. (2006). Gialpha and Gbeta subunits both define selectivity of G protein activation by alpha2-adrenergic receptors. Proc. Natl. Acad. Sci. USA *103*, 212–217.

Gilman, A.G. (1987). G proteins: transducers of receptor-generated signals. Annu. Rev. Biochem. *56*, 615–649.

Hall, M.P., Unch, J., Binkowski, B.F., Valley, M.P., Butler, B.L., Wood, M.G., Otto, P., Zimmerman, K., Vidugiris, G., Machleidt, T., et al. (2012). Engineered luciferase reporter from a deep sea shrimp utilizing a novel imidazopyrazinone substrate. ACS Chem. Biol. *7*, 1848–1857.

Harding, S.D., Sharman, J.L., Faccenda, E., Southan, C., Pawson, A.J., Ireland, S., Gray, A.J.G., Bruce, L., Alexander, S.P.H., Anderton, S., et al.; NC-IUPHAR (2018). The IUPHAR/BPS Guide to PHARMACOLOGY in 2018: updates and expansion to encompass the new guide to IMMUNOPHARMACOLOGY. Nucleic Acids Res. *46* (D1), D1091–D1106.

Hollins, B., Kuravi, S., Digby, G.J., and Lambert, N.A. (2009). The c-terminus of GRK3 indicates rapid dissociation of G protein heterotrimers. Cell. Signal. *21*, 1015–1021.

Ishii, K., Hein, L., Kobilka, B., and Coughlin, S.R. (1993). Kinetics of thrombin receptor cleavage on intact cells. Relation to signaling. J. Biol. Chem. *268*, 9780–9786.

Janetopoulos, C., Jin, T., and Devreotes, P. (2001). Receptor-mediated activation of heterotrimeric G-proteins in living cells. Science *291*, 2408–2411.

Johnston, C.A., Lobanova, E.S., Shavkunov, A.S., Low, J., Ramer, J.K., Blaesius, R., Fredericks, Z., Willard, F.S., Kuhlman, B., Arshavsky, V.Y., and Siderovski, D.P. (2006). Minimal determinants for binding activated G alpha from the structure of a G alpha(i1)-peptide dimer. Biochemistry *45*, 11390–11400.

Johnston, C.A., Willard, F.S., Ramer, J.K., Blaesius, R., Roques, C.N., and Siderovski, D.P. (2008). State-selective binding peptides for heterotrimeric G-protein subunits: novel tools for investigating G-protein signaling dynamics. Comb. Chem. High Throughput Screen. *11*, 370–381.

Kaech, S., and Banker, G. (2006). Culturing hippocampal neurons. Nature Protocols *1*, 2406–2415.

Kimple, R.J., Kimple, M.E., Betts, L., Sondek, J., and Siderovski, D.P. (2002). Structural determinants for GoLoco-induced inhibition of nucleotide release by Galpha subunits. Nature *416*, 878–881.

Koch, W.J., Hawes, B.E., Allen, L.F., and Lefkowitz, R.J. (1994). Direct evidence that Gi-coupled receptor stimulation of mitogen-activated protein kinase is mediated by G beta gamma activation of p21ras. Proc. Natl. Acad. Sci. USA *91*, 12706–12710.

Lambert, N.A., Johnston, C.A., Cappell, S.D., Kuravi, S., Kimple, A.J., Willard, F.S., and Siderovski, D.P. (2010). Regulators of G-protein signaling accelerate GPCR signaling kinetics and govern sensitivity solely by accelerating GTPase activity. Proc. Natl. Acad. Sci. USA *107*, 7066–7071.

Lan, K.L., Sarvazyan, N.A., Taussig, R., Mackenzie, R.G., DiBello, P.R., Dohlman, H.G., and Neubig, R.R. (1998). A point mutation in Galphao and Galphai1 blocks interaction with regulator of G protein signaling proteins. J. Biol. Chem. *273*, 12794–12797.

Landis, C.A., Masters, S.B., Spada, A., Pace, A.M., Bourne, H.R., and Vallar, L. (1989). GTPase inhibiting mutations activate the alpha chain of Gs and stimulate adenylyl cyclase in human pituitary tumours. Nature *340*, 692–696.

Lee, M.H., Appleton, K.M., Strungs, E.G., Kwon, J.Y., Morinelli, T.A., Peterson, Y.K., Laporte, S.A., and Luttrell, L.M. (2016). The conformational signature of β-arrestin2 predicts its trafficking and signalling functions. Nature *531*, 665–668.

Levitt, E.S., Purington, L.C., and Traynor, J.R. (2011). Gi/o-coupled receptors compete for signaling to adenylyl cyclase in SH-SY5Y cells and reduce opioid-mediated cAMP overshoot. Mol. Pharmacol. *79*, 461–471.

Leyme, A., Marivin, A., Perez-Gutierrez, L., Nguyen, L.T., and Garcia-Marcos, M. (2015). Integrins activate trimeric G proteins via the nonreceptor protein GIV/Girdin. J. Cell Biol. *210*, 1165–1184.

Leyme, A., Marivin, A., Maziarz, M., DiGiacomo, V., Papakonstantinou, M.P., Patel, P.P., Blanco-Canosa, J.B., Walawalkar, I.A., Rodriguez-Davila, G., Dominguez, I., and Garcia-Marcos, M. (2017). Specific inhibition of GPCR-independent G protein signaling by a rationally engineered protein. Proc. Natl. Acad. Sci. USA *114*, E10319–E10328.

Lohse, M.J., Nuber, S., and Hoffmann, C. (2012). Fluorescence/bioluminescence resonance energy transfer techniques to study G-protein-coupled receptor activation and signaling. Pharmacol. Rev. *64*, 299–336.

Longo, P.A., Kavran, J.M., Kim, M.S., and Leahy, D.J. (2013). Transient mammalian cell transfection with polyethylenimine (PEI). Methods Enzymol. *529*, 227–240.

Lyons, J., Landis, C.A., Harsh, G., Vallar, L., Grünewald, K., Feichtinger, H., Duh, Q.Y., Clark, O.H., Kawasaki, E., Bourne, H.R., et al. (1990). Two G protein oncogenes in human endocrine tumors. Science *249*, 655–659.

Marivin, A., Leyme, A., Parag-Sharma, K., DiGiacomo, V., Cheung, A.Y., Nguyen, L.T., Dominguez, I., and Garcia-Marcos, M. (2016). Dominant-negative Gα subunits are a mechanism of dysregulated heterotrimeric G protein signaling in human disease. Sci. Signal. *9*, ra37.

Masuho, I., Ostrovskaya, O., Kramer, G.M., Jones, C.D., Xie, K., and Martemyanov, K.A. (2015). Distinct profiles of functional discrimination among G proteins determine the actions of G protein-coupled receptors. Sci. Signal. *8*, ra123.

Maziarz, M., Broselid, S., DiGiacomo, V., Park, J.C., Luebbers, A., Garcia-Navarrete, L., Blanco-Canosa, J.B., Baillie, G.S., and Garcia-Marcos, M. (2018a). A biochemical and genetic discovery pipeline identifies PLCδ4b as a nonreceptor activator of heterotrimeric G-proteins. J. Biol. Chem. *293*, 16964–16983.

Maziarz, M., Leyme, A., Marivin, A., Luebbers, A., Patel, P.P., Chen, Z., Sprang, S.R., and Garcia-Marcos, M. (2018b). Atypical activation of the G protein $G\alpha_q$ by the oncogenic mutation Q209P. J. Biol. Chem. *293*, 19586–19599.

Nuber, S., Zabel, U., Lorenz, K., Nuber, A., Milligan, G., Tobin, A.B., Lohse, M.J., and Hoffmann, C. (2016). β-Arrestin biosensors reveal a rapid, receptor-dependent activation/deactivation cycle. Nature *531*, 661–664.

O'Hayre, M., Vazquez-Prado, J., Kufareva, I., Stawiski, E.W., Handel, T.M., Seshagiri, S., and Gutkind, J.S. (2013). The emerging mutational landscape of G proteins and G-protein-coupled receptors in cancer. Nat. Rev. Cancer *13*, 412–424.

O'Hayre, M., Inoue, A., Kufareva, I., Wang, Z., Mikelis, C.M., Drummond, R.A., Avino, S., Finkel, K., Kalim, K.W., DiPasquale, G., et al. (2016). Inactivating mutations in GNA13 and RHOA in Burkitt's lymphoma and diffuse large B-cell lymphoma: a tumor suppressor function for the Gα13/RhoA axis in B cells. Oncogene *35*, 3771–3780.

Oner, S.S., An, N., Vural, A., Breton, B., Bouvier, M., Blumer, J.B., and Lanier, S.M. (2010). Regulation of the AGS3·Galphai signaling complex by a seven-transmembrane span receptor. J. Biol. Chem. *285*, 33949–33958.

Pace, A.M., Wong, Y.H., and Bourne, H.R. (1991). A mutant alpha subunit of Gi2 induces neoplastic transformation of Rat-1 cells. Proc. Natl. Acad. Sci. USA *88*, 7031–7035.

Parag-Sharma, K., Leyme, A., DiGiacomo, V., Marivin, A., Broselid, S., and Garcia-Marcos, M. (2016). Membrane Recruitment of the Non-receptor Protein GIV/Girdin (Gα-interacting, Vesicle-associated Protein/Girdin) Is Sufficient for Activating Heterotrimeric G Protein Signaling. J. Biol. Chem. *291*, 27098–27111.

Qin, K., Dong, C., Wu, G., and Lambert, N.A. (2011). Inactive-state preassembly of G(q)-coupled receptors and G(q) heterotrimers. Nat. Chem. Biol. *7*, 740–747.

Ritt, M., Guan, J.L., and Sivaramakrishnan, S. (2013). Visualizing and manipulating focal adhesion kinase regulation in live cells. J. Biol. Chem. *288*, 8875–8886.

Ross, E.M., and Wilkie, T.M. (2000). GTPase-activating proteins for heterotrimeric G proteins: regulators of G protein signaling (RGS) and RGS-like proteins. Annu. Rev. Biochem. *69*, 795–827.

Sakurai, K., Zhao, S., Takatoh, J., Rodriguez, E., Lu, J., Leavitt, A.D., Fu, M., Han, B.X., and Wang, F. (2016). Capturing and Manipulating Activated Neuronal Ensembles with CANE Delineates a Hypothalamic Social-Fear Circuit. Neuron *92*, 739–753.

Sato, M., Blumer, J.B., Simon, V., and Lanier, S.M. (2006). Accessory proteins for G proteins: partners in signaling. Annu. Rev. Pharmacol. Toxicol. *46*, 151–187.

Schneider, C.A., Rasband, W.S., and Eliceiri, K.W. (2012). NIH Image to ImageJ: 25 years of image analysis. Nature Methods *9*, 671–675.

Shirley, M.D., Tang, H., Gallione, C.J., Baugher, J.D., Frelin, L.P., Cohen, B., North, P.E., Marchuk, D.A., Comi, A.M., and Pevsner, J. (2013). Sturge-Weber syndrome and port-wine stains caused by somatic mutation in GNAQ. N. Engl. J. Med. *368*, 1971–1979.

Siderovski, D.P., and Willard, F.S. (2005). The GAPs, GEFs, and GDIs of heterotrimeric G-protein alpha subunits. Int. J. Biol. Sci. *1*, 51–66.

Sivaramakrishnan, S., and Spudich, J.A. (2011). Systematic control of protein interaction using a modular ER/K α-helix linker. Proc. Natl. Acad. Sci. USA *108*, 20467–20472.

Sriram, K., and Insel, P.A. (2018). GPCRs as targets for approved drugs: How many targets and how many drugs? Mol. Pharmacol. *93*, 251–258.

Sterne-Marr, R., Tesmer, J.J., Day, P.W., Stracquatanio, R.P., Cilente, J.A., O'Connor, K.E., Pronin, A.N., Benovic, J.L., and Wedegaertner, P.B. (2003). G protein-coupled receptor Kinase 2/G alpha q/11 interaction. A novel surface on a regulator of G protein signaling homology domain for binding G alpha subunits. J. Biol. Chem. *278*, 6050–6058.

Swanson, C.J., and Sivaramakrishnan, S. (2014). Harnessing the unique structural properties of isolated α-helices. J. Biol. Chem. *289*, 25460–25467.

Tall, G.G. (2013). Ric-8 regulation of heterotrimeric G proteins. J. Recept. Signal Transduct. Res. *33*, 139–143.

Tall, G.G., Krumins, A.M., and Gilman, A.G. (2003). Mammalian Ric-8A (synembryn) is a heterotrimeric Galpha protein guanine nucleotide exchange factor. J. Biol. Chem. *278*, 8356–8362.

Tang, Y., Hu, L.A., Miller, W.E., Ringstad, N., Hall, R.A., Pitcher, J.A., DeCamilli, P., and Lefkowitz, R.J. (1999). Identification of the endophilins (SH3p4/p8/p13) as novel binding partners for the beta1-adrenergic receptor. Proc. Natl. Acad. Sci. USA *96*, 12559–12564.

Tesmer, V.M., Kawano, T., Shankaranarayanan, A., Kozasa, T., and Tesmer, J.J. (2005). Snapshot of activated G proteins at the membrane: the Galphaq-GRK2-Gbetagamma complex. Science *310*, 1686–1690.

Van Raamsdonk, C.D., Bezrookove, V., Green, G., Bauer, J., Gaugler, L., O'Brien, J.M., Simpson, E.M., Barsh, G.S., and Bastian, B.C. (2009). Frequent somatic mutations of GNAQ in uveal melanoma and blue naevi. Nature *457*, 599–602.

Voyno-Yasenetskaya, T.A., Pace, A.M., and Bourne, H.R. (1994). Mutant alpha subunits of G12 and G13 proteins induce neoplastic transformation of Rat-1 fibroblasts. Oncogene *9*, 2559–2565.

Webb, C.K., McCudden, C.R., Willard, F.S., Kimple, R.J., Siderovski, D.P., and Oxford, G.S. (2005). D2 dopamine receptor activation of potassium channels is selectively decoupled by Galpha-specific GoLoco motif peptides. J. Neurochem. *92*, 1408–1418.

Weis, W.I., and Kobilka, B.K. (2018). The Molecular Basis of G Protein-Coupled Receptor Activation. Annu. Rev. Biochem. *87*, 897–919.

Wells, C.D., Gutowski, S., Bollag, G., and Sternweis, P.C. (2001). Identification of potential mechanisms for regulation of p115 RhoGEF through analysis of endogenous and mutant forms of the exchange factor. J. Biol. Chem. *276*, 28897–28905.

Wells, C., Jiang, X., Gutowski, S., and Sternweis, P.C. (2002). Functional characterization of p115 RhoGEF. Methods Enzymol. *345*, 371–382.

Willard, F.S., Kimple, R.J., and Siderovski, D.P. (2004). Return of the GDI: the GoLoco motif in cell division. Annu. Rev. Biochem. *73*, 925–951.

Wisler, J.W., Rockman, H.A., and Lefkowitz, R.J. (2018). Biased G Protein-Coupled Receptor Signaling: Changing the Paradigm of Drug Discovery. Circulation *137*, 2315–2317.

Xu, N., Voyno-Yasenetskaya, T., and Gutkind, J.S. (1994). Potent transforming activity of the G13 alpha subunit defines a novel family of oncogenes. Biochem. Biophys. Res. Commun. *201*, 603–609.

Yost, E.A., Mervine, S.M., Sabo, J.L., Hynes, T.R., and Berlot, C.H. (2007). Live cell analysis of G protein beta5 complex formation, function, and targeting. Mol. Pharmacol. *72*, 812–825.

Please cite this article in press as: Maziarz et al., Revealing the Activity of Trimeric G-proteins in Live Cells with a Versatile Biosensor Design, Cell (2020), https://doi.org/10.1016/j.cell.2020.06.020

STAR★METHODS

KEY RESOURCES TABLE

REAGENT or RESOURCE	SOURCE	IDENTIFIER
Antibodies		
Rabbit polyclonal anti-pan-Gβ (M-14)	Santa Cruz Biotechnology	Cat# sc-261; RRID:AB_63154
Rabbit polyclonal anti-Gαi3 (C-10)	Santa Cruz Biotechnology	Cat# sc-262; RRID:AB_2279066
Rabbit polyclonal anti-Gαq (E-17)	Santa Cruz Biotechnology	Cat# sc-393; RRID:AB_631536
mouse monoclonal anti-Gαo (A-2)	Santa Cruz Biotechnology	Cat# sc-13532; RRID:AB_2111645
mouse monoclonal anti-Gαs (12)	Santa Cruz Biotechnology	Cat# sc-135914; RRID:AB_2111662
Mouse monoclonal anti-α-tubulin	Sigma-Aldrich	Cat# T6074; RRID:AB_477582
Rabbit polyclonal anti-Nanoluciferase	L. Encell (Promega) (Hall et al., 2012)	N/A
Rabbit polyclonal anti-RFP	Rockland Immunochemicals	Cat# 600-401-379; RRID:AB_2209751
Mouse monoclonal anti-hemagglutinin (HA) tag (clone 12CA5)	Roche	Cat# 11583816001; RRID:AB_514505
Mouse monoclonal anti-GFP (JL-8)	Clontech / Takara Bio	Cat# 632380; RRID:AB_10013427
Rabbit polyclonal anti-Gαi3	Aviva Systems Biology	cat# OAAB19207
Rabbit monoclonal anti-phospho-ERK1/2 (T202/ Y204)	Cell Signaling Technologies	Cat# 4370; RRID:AB_2315112
Rabbit polyclonal anti-ERK1/2	Cell Signaling Technologies	Cat# 9102; RRID:AB_330744
Rabbit polyclonal anti-Gαi1/2/3	Cell Signaling Technologies	Cat# 5290; RRID:AB_190398
mouse monoclonal anti-Myc epitope (clone 9B11)	Cell Signaling Technologies	Cat# 2276; RRID:AB_331783
Mouse monoclonal anti-GFP	Santa Cruz Biotechnology	Cat# sc-9996; RRID:AB_627695
Goat anti-rabbit Alexa Fluor 680	Invitrogen	Cat# A-21077; RRID:AB_2535737
goat anti-mouse IRDye 800	LI-COR	Cat# 926-32210; RRID:AB_621842
goat anti-mouse Alexa Fluor 488	Invitrogen	Cat# A-11017; RRID:AB_2534084
Bacterial and Virus Strains		
NEB 5-alpha competent *E. coli*	NEB	Cat# C2987I
BL21(DE3) Chemically Competent *E. coli*	Invitrogen	Cat# C600003
Chemicals, Peptides, and Recombinant Proteins		
Brimonidine	Ark Pharm	Cat# AK-35795
Yohimbine	Alfa Aesar	Cat# J60185
Atropine	Alfa Aesar	Cat# A10236
DL-isoproterenol hydrochloride	Alfa Aesar	Cat# J61788
Rapamycin	Alfa Aesar	Cat# J62473
Carbachol	Acros Organics	Cat# AC-10824
Adenosine	Acros Organics	Cat# 164040050
DAMGO	Tocris	Cat# 1171
DADLE	Tocris	Cat# 3790
naloxone hydrochloride	Tocris	Cat# 0599
(R)-(-)-phenylephrine	Tocris	Cat# 2838
SCH-79797 dihydrochloride	Tocris	Cat# 1592
Forskolin	Tocris	Cat# 1099
(R)-Baclofen	Tocris	Cat# 0796
CGP 54626 hydrochloride	Tocris	Cat# 1088
NECA	Tocris	Cat# 1691
(S)-3,5-DHPG	Tocris	Cat# 0805
DPCPX	Tocris	Cat# 0439
Thrombin Receptor Activator Peptide 6 (TRAP-6)	Anaspec	Cat# AS-24190

(*Continued on next page*)

Please cite this article in press as: Maziarz et al., Revealing the Activity of Trimeric G-proteins in Live Cells with a Versatile Biosensor Design, Cell (2020), https://doi.org/10.1016/j.cell.2020.06.020

Continued

REAGENT or RESOURCE	SOURCE	IDENTIFIER
Human alpha-thrombin	Haematologic Technologies	Cat# HCT-0020
SNC-80	Calbiochem	Cat# 508161
Pertussis toxin	List Biologicals	Cat# 179A
YM-254890	Wako Chemical	Cat# 257-00631
Q5 DNA polymerase	New England Biolabs	Cat# M0491L
PfuUltra DNA polymerase	Agilent	Cat# 600380
SigmaFAST protease inhibitor cocktail	Sigma	Cat# S8830
Critical Commercial Assays		
NanoGlo Luciferase Assay System	Promega	Cat# N1120
Dual-Glo Luciferase Assay System	Promega	Cat# E2920
LANCE cAMP kit	PerkinElmer	Cat# AD0262
QuikChange II Site-Directed Mutagenesis Kit	Agilent	Cat# #200523
Deposited Data		
Mendeley dataset (Gαi immunoblots)	This paper	Mendeley Data: https://doi.org/10.17632/n3s5g457fm.1
Experimental Models: Cell Lines		
Human: 293T	ATCC	Cat# CRL-3216
Human: HeLa	ATCC	Cat# CCL-2
Human: SH-SY5Y	ATCC	Cat# CRL-2266
Human: Lenti-X 293T	Takara Bio	Cat# 632180
Experimental Models: Organisms/Strains		
Mouse: C57BL/6	Charles River	Strain code: 027
Recombinant DNA		
pcDNA3-$\alpha 2_{A/D}$-AR	S.M. Lanier and J. Blumer (Medical University of South Carolina) (Oner et al., 2010)	N/A
pcDNA3.1-3xHA-M3R	cDNA Resource Center	cat# MAR030TN00
pcDNA3.1-3xHA-M4R	cDNA Resource Center	cat# MAR040TN00
pcDNA3.1-3xHA-ADRA1A	cDNA Resource Center	cat# AR0A1ATN00
pcDNA3.1(-) 3xHA-RGS8	cDNA Resource Center	cat# RGS080TN00
pcDNA3.1-Gα13(EE)	cDNA Resource Center	cat# GNA130EI00
pcDNA3.1-Gαs (short)	cDNA Resource Center	cat# GNA0SS0000
pcDNA3.1-Gαq-YFP (Venus variant)	N. Lambert (Augusta University) (Qin et al., 2011).	N/A
pcDNA3.1-Gαq-YFP (Venus variant) Q209L	Maziarz et al., 2018b	N/A
pcDNA3.1-Gαq-YFP (Venus variant) R183C	This paper	N/A
pcDNA3.1-Gαq-YFP (Venus variant) R247Q	This paper	N/A
pcDNA3.1-Gαq-YFP (Venus variant) R247L	This paper	N/A
pcDNA3.1-$G\beta_1$,	N. Lambert (Augusta University) (Hollins et al., 2009)	N/A
pcDNA3.1-$G\gamma_2$	N. Lambert (Augusta University) (Hollins et al., 2009)	N/A
pcDNA3.1-Venus(1-155)-$G\gamma_2$ (VN-$G\gamma_2$)	N. Lambert (Augusta University) (Hollins et al., 2009)	N/A
pcDNA3.1- Venus(155-239)-$G\beta_1$ (VC-$G\beta_1$)	N. Lambert (Augusta University) (Hollins et al., 2009)	N/A
pcDNA3.1-MOR-FLAG	K. Martemyanov (Scripps Res. Inst.,FL) (Masuho et al., 2015)	N/A
pcDNA3.1-masGRK3ct-NanoLuc	K. Martemyanov (Scripps Res. Inst.,FL) (Masuho et al., 2015)	N/A

(*Continued on next page*)

Please cite this article in press as: Maziarz et al., Revealing the Activity of Trimeric G-proteins in Live Cells with a Versatile Biosensor Design, Cell (2020), https://doi.org/10.1016/j.cell.2020.06.020

Continued

REAGENT or RESOURCE	SOURCE	IDENTIFIER
pcDNA3 Flag beta-2-adrenergic receptor	Tang et al., 1999	Addgene cat #14697
G protein alpha-s-YFP	Yost et al., 2007	Addgene cat #55781
G protein alpha-o-YFP	Yost et al., 2007	Addgene cat #55776
pBJ-FLAG-hPAR1	Ishii et al., 1993	Addgene cat #53226
pcDNA3.1(-)-Gαi3-YFP (Citrine variant, b/c loop insert)	Marivin et al., 2016	N/A
pGEX-KG-GAIP	De Vries et al., 1995	N/A
pGL3-SRE.L	R. Neubig (Michigan State University) (Wells et al., 2001)	N/A
pCMV-Beta	Clontech	cat# 631719
pcDNA3.1(+)-Gαo	Garcia-Marcos et al., 2011	N/A
pcDNA3-Gαi3	Ghosh et al., 2008	N/A
p3XFLAG-CMV14-Gαi3 C351I	This paper	N/A
pmRFP-FKBP-Ric8A	This paper	N/A
pcDNA3.1-mas-KB-1753-Nluc	This paper	N/A
pcDNA3.1-mas-KB-1753-Nluc I9A/W10A	This paper	N/A
pcDNA3.1-mas-GRK2^{RH}-Nluc	This paper	N/A
pcDNA3.1-mas-GRK2^{RH}-Nluc L118A	This paper	N/A
pcDNA3.1-mas-p115^{RH}-Nluc	This paper	N/A
pcDNA3.1-mas-PRG^{RH}-Nluc	This paper	N/A
pcDNA3.1-Gα13(EE)-YFP	This paper	N/A
pcDNA3.1-Gα13(EE)-YFP Q226L	This paper	N/A
pcDNA3.1-Gα13(EE)-YFP R200K	This paper	N/A
pcDNA3.1-Gα13(EE)-YFP R200G	This paper	N/A
pmRFP-FKBP-RGS12-GL	This paper	N/A
Lyn11-FRB	Parag-Sharma et al., 2016	N/A
pcDNA3.1-Gαi*-BERKY1	This paper	N/A
pcDNA3.1-Gαi*-BERKY2	This paper	N/A
pcDNA3.1-Gαi*-BERKY3	This paper	N/A
pcDNA3.1-KB-1746-BERKY3	This paper	N/A
pcDNA3.1-Gαq*-BERKY3	This paper	N/A
pcDNA3.1-Gα13*-BERKY3	This paper	N/A
pcDNA3.1-Gβγ-BERKY3	This paper	N/A
pcDNA3.1-Rho*-BERKY3	This paper	N/A
pLVX-IRES-Gαi*-BERKY3	This paper	N/A
pLVX-IRES-Gαq*-BERKY3	This paper	N/A
pLVX-IRES-Gβγ-BERKY3	This paper	N/A
pLenti-hSyn-Gαi*-BERKY1	This paper	N/A
pLenti-hSyn-Gαi*-BERKY3	This paper	N/A
pLenti-hSynapsin-Cre-WPRE	Sakurai et al., 2016	Addgene cat# 86641
pLenti-hSyn-Gβγ-BERKY1	This paper	N/A
pLenti-hSyn-Gαq*-BERKY1	This paper	N/A
Software and Algorithms		
GraphPad Prism	GraphPad Software	https://www.graphpad.com/scientific-software/prism/
ImageJ	Schneider et al., 2012	https://imagej.nih.gov/ij/
Adobe Photoshop	Adobe	https://www.adobe.com/
Adobe Illustrator	Adobe	https://www.adobe.com/
ICM	Molsoft LLC	http://www.molsoft.com/

Please cite this article in press as: Maziarz et al., Revealing the Activity of Trimeric G-proteins in Live Cells with a Versatile Biosensor Design, Cell (2020), https://doi.org/10.1016/j.cell.2020.06.020

RESOURCE AVAILABILITY

Lead Contact

Further information and requests for resources and reagents should be directed to and will be fulfilled by the Lead Contact, Mikel Garcia-Marcos (mgm1@bu.edu).

Materials Availability

All unique reagents generated in this study are available from the Lead Contact but we may require a completed Materials Transfer Agreement if there is potential for commercial application.

Data and Code Availability

Original data for Gαi immunoblots in the paper have been deposited to Mendeley Data: https://doi.org/10.17632/n3s5g457fm.1.

EXPERIMENTAL MODEL AND SUBJECT DETAILS

Cell lines

HEK293T cells (ATCC cat# CRL-3216,) and HeLa cells (ATCC cat# CCL-2) were grown at 37°C, 5% CO_2 in DMEM supplemented with 10% FBS, 100 U/ml penicillin, 100 μg/ml streptomycin, and 1% L-glutamine. SH-SY5Y cells (ATCC cat# CRL-2266) were grown at 37°C, 5% CO_2 in DMEM supplemented with 100 U/ml penicillin, 100 μg/ml streptomycin, 1% L-glutamine, and 15% heat-inactivated FBS.

Mouse primary cortical neuron culture

Cortical neurons were isolated from neonatal mouse (C57BL/6, Charles River, Strain code 027) brains as previously described (Kaech and Banker, 2006) with modifications. All animal procedures were approved by the Institutional Animal Care and Use Committee (IACUC) at Boston University School of Medicine. Newborn mouse pups (P0) were euthanized by decapitation, brains removed from the skull, and placed in cold HBSS. The cerebrum was detached from other brain regions under a stereomicroscope by removal of the olfactory bulb and cerebellum, the brain removed from the meninges and separated into hemispheres, and the cortex dissected out with forceps. The cortex was minced into approximately 1-2 mm pieces using a sterile razor blade, and digested with 0.05% Trypsin in HBSS for 10 min at 37°C. Trypsinized tissue was washed three times with HBSS to remove trypsin, and resuspended in DMEM supplemented with 10% FBS, 100 U/ml penicillin, 100 μg/ml streptomycin, and 1% L-glutamine (complete DMEM) before passing through a sterile 40 μm cell strainer (Fisherbrand, cat# 22363547) to obtain a cell suspension. Approximately 50,000-75,000 cells were plated on 5 mm diameter coverslips (coated overnight with 0.1 mg/mL poly-L-lysine hydrobromide, and washed 3x with HBSS) and placed in 96-well plates containing complete DMEM for 4 h, before replacing one half of the media with Neurobasal media (GIBCO, cat# 21103049) with B-27 supplement (GIBCO, cat# 17504001) and 1x Glutamax-I (GIBCO, cat# 35050061) (complete neural medium). On day *in vitro* 3 (DIV3), one half of the media was replaced with complete neural media supplemented with 5 μM AraC. Beginning DIV5, half of the media was replaced by fresh complete neural medium every other day.

METHOD DETAILS

Plasmids

The plasmid encoding KB-1753-Nluc (pcDNA3.1-mas-KB-1753-Nluc) was generated by replacing the GRK3ct sequence of pcDNA3.1-mas-GRK3ct-NanoLuc (Masuho et al., 2015) by digestion with HindIII/BamHI and subsequent insertion of the KB-1753 sequence (SSRGYYHGIWVGEEGRLSR) flanked with a Gly-Gly linker on each end. A similar approach was followed to generate the plasmids encoding $GRK2^{RH}$-Nluc (pcDNA3.1-mas$GRK2^{RH}$-Nluc), $p115^{RH}$-Nluc (pcDNA3.1-mas-$p115^{RH}$-Nluc) and PRG^{RH}-Nluc (pcDNA3.1-mas-PRG^{RH}-Nluc). Essentially, the RGS homology (RH) domain from bovine GRK2 (aa 45-178), human p115-RhoGEF (aa 43-250, RH domain lacking the N-terminal extension that confers GAP activity (Chen et al., 2003)) or rat PDZ-RhoGEF (aa 307-508) replaced the position originally used by the GRK3ct cassette in pcDNA3.1-masGRK3ct-NanoLuc. Plasmids encoding untagged and split Venus-tagged Gβ1 and Gγ2 (pcDNA3.1-$G\beta_1$, pcDNA3.1-$G\gamma_2$, pcDNA3.1-Venus(155-239)-$G\beta_1$, pcDNA3.1-Venus(1-155)-$G\gamma_2$) have been described previously (Hollins et al., 2009). Plasmids encoding Gαq-YFP (wild-type and Q209P mutant) and Gαi3-YFP have been described previously (Marivin et al., 2016; Maziarz et al., 2018b; Qin et al., 2011), and plasmids encoding YFP-tagged Gαs and Gαo were obtained from Addgene (Yost et al., 2007). Plasmids encoding untagged Gαi3 and untagged Gαo have been described previously (Garcia-Marcos et al., 2011; Ghosh et al., 2008). Plasmid pcDNA3.1-Gα13(EE)-YFP encoding Gα13 internally-tagged with the Citrine variant of YFP in the b/c loop was generated by first introducing a SacII restriction site after amino acid P131 into pcDNA3.1-Gα13(EE) and then inserting Citrine, flanked by a GSG linker on each end, at this site by Gibson assembly. The plasmid encoding $\alpha2_A$-AR (pcDNA3-$\alpha2_{A/D}$-AR) has been described previously (Oner et al., 2010) and the plasmids for β2-AR (Tang et al., 1999) and PAR1 (Ishii et al., 1993) were obtained from Addgene. Plasmid pmRFP-FKBP-RGS12-GL encoding FKBP-R12-GoLoco was constructed by replacing the pseudojanin sequence between the NruI/BamHI sites of pmRFP-FKBP-pseudojanin (Addgene, #37999) by mouse RGS12 amino acids 1185-1221 (DEAEEFFELISKAQSNRADDQRGLLRKEDLVLPEFLR).

Please cite this article in press as: Maziarz et al., Revealing the Activity of Trimeric G-proteins in Live Cells with a Versatile Biosensor Design, Cell (2020), https://doi.org/10.1016/j.cell.2020.06.020

Plasmid pmRFP-FKBP-Ric-8A encoding Ric-8A tagged with RFP and FKBP was constructed by replacing the pseudojanin sequence between the NruI/BamHI sites of pmRFP-FKBP-pseudojanin (Addgene, #37999) by rat Ric-8A amino acids 12-492. The plasmid encoding Lyn11-FRB has been described previously (Parag-Sharma et al., 2016). The plasmid encoding the pertussis toxin insensitive C351I mutant of Gαi3 (p3xFLAG-CMV-14-Gαi3 C351I) was generated by mutating codon 351 and by placing a stop codon before the 3XFLAG tag of p3xFLAG-CMV-14-Gαi3 (Garcia-Marcos et al., 2010). The plasmid for the bacterial expression of GST-fused GAIP (pGEX-KG-GAIP) has been described previously (De Vries et al., 1995). Plasmids encoding M3R, M4R, RGS8, Gα13(EE) and Gαs (pcDNA3.1-3xHA-M3R, pcDNA3.1-3xHA-M4R, pcDNA3.1-3xHA-ADRA1A, pcDNA3.1(-) 3xHA-RGS8, pcDNA3.1-Gα13(EE), and pcDNA3.1-Gαs (short)) were obtained from the cDNA Resource Center at Bloomsburg University. The plasmids encoding MOR (pcDNA3.1-MOR-FLAG) has been described previously (Masuho et al., 2015).

Plasmids encoding BERKY biosensors were generated sequentially from a synthetic DNA fragment containing the following elements (from N- to C terminus of the protein sequence): Lyn11 / Nluc / ER/K α-helix / YFP (Citrine variant) / KB-1753 / myc-tag. Each of these elements was separated by glycine-rich linkers and unique restriction sites, and the ER/K α-helix sequence was obtained from pcDNA-FRT-FAK-kinase10 (Addgene #59123) (Ritt et al., 2013). A full sequence of this and other BERKY constructs is provided in Data S1. This synthetic DNA was inserted between the NheI/XbaI sites in pcDNA3.1(+) to generate pcDNA3.1-Gαi*-BERKY1. pcDNA3.1-Gαi*-BERKY2 and pcDNA3.1-Gαi*-BERKY3 were generated sequentially by inserting a first YFP into a BamHI site of Gαi*-BERKY1 and a second one into the AscI site of Gαi*-BERKY2. Plasmid pcDNA3.1-KB-1746-BERKY3 was constructed by inserting the KB-1746 sequence (SSSYSEHCQRWGCYARLSR) into XhoI-digested pcDNA3.1-Gαi*-BERKY3 by Gibson assembly, which results in the replacement of the KB-1753 sequence. Plasmids pcDNA3.1-Gαq*-BERKY3, pcDNA3.1-Gα13*-BERKY3, pcDNA3.1-Gβγ-BERKY3, and pcDNA3.1-Rho*-BERKY3 were generated by inserting $GRK2^{RH}$, PRG^{RH}, GRK3ct, or Rhotekin's RBD (amino acids 7-89), respectively, followed by a stop codon into XhoI-digested pcDNA3.1-Gαi*-BERKY3, which results in the replacement of the KB-1753 sequence and myc tag. Lentiviral plasmids encoding Gαi*-BERKY3 (pLVX-IRES-Gαi*-BERKY3), Gαq*-BERKY3 (pLVX-IRES-Gαq*-BERKY3), and Gβγ-BERKY3 (pLVX-IRES-Gβγ-BERKY3) under the control of the CMV promoter were generated by PCR amplification from their respective pcDNA3.1-based plasmids (including NheI/XbaI flanking sites that remained intact in the final construct) and insertion into the XhoI site of pLVX-IRES-Hyg (Clontech, cat# 632185) by Gibson assembly. The lentiviral constructs encoding Gαi*-BERKY1 and Gαi*-BERKY3 under the control of human synapsin (hSyn) promoter (pLenti-hSyn-Gαi*-BERKY1 and pLenti-hSyn-Gαi*-BERKY3, respectively) were constructed by inserting the respective NheI-XbaI fragment from pcDNA3.1-Gαi*-BERKY1 or pcDNA3.1-Gαi*-BERKY3 (encompassing the entire biosensor sequence) between the AgeI and EcoRI sites of pLenti-hSynapsin-Cre-WPRE (Addgene #86641; Sakurai et al., 2016) by Gibson assembly, such that both sites were destroyed and replaced by NheI/GCCACC in the 5′ end and XbaI/AgeI in the 3′ end, respectively. The lentiviral construct encoding Gβγ-BERKY1 (pLenti-hSyn-Gβγ-BERKY1) was designed by inserting the GRK3ct coding sequence followed by a stop codon between the AgeI sites of pLenti-hSyn-Gαi*-BERKY1, which results in the replacement of the KB-1753 sequence and myc tag. The construct encoding Gαq*-BERKY1 (pLenti-hSyn-Gαq*-BERKY1) was designed in two steps. First, $GRK2^{RH}$ followed by a stop codon was inserted into XhoI-digested pcDNA3.1-Gαi*-BERKY1 to generate pcDNA3.1-Gαq*-BERKY1, which was then used to transfer the biosensor sequence flanked by NheI and XbaI into pLenti-hSynapsin-Cre-WPRE using an approach analogous to that described above for pLenti-hSyn-Gβγ-BERKY1. All plasmids were purified from DH5α bacteria. All point mutations were generated using QuikChange II (Agilent, #200523).

Bioluminescence Resonance Energy Transfer (BRET) measurements in HEK293T and SH-SY5Y cells

HEK293T cells were seeded on 6-well plates (~400,000 cells/well) coated with 0.1% gelatin, transfected ~24 h later using the calcium phosphate method. For experiments with bi-molecular biosensors consisting of YFP-tagged Gα proteins and Nluc-fused detector modules (Figures 1, 2, 4, and 5; Figures S1 and S3–S5), cells were transfected with the following amounts of plasmid DNA per well of the constructs indicated in the corresponding figures: 0.5-1 μg for Gαi3-YFP, Gαq-YFP (except in Figure S2A, which was 0.25 μg), Gαs-YFP, Gαo-YFP or Gα13-YFP, 0.025-0.2 μg for mas-KB-1753-Nluc, and 0.05-0.2 μg for mas-$GRK2^{RH}$-Nluc, mas-$p115^{RH}$-Nluc and mas-PRG^{RH}-Nluc. Essentially, optimal donor: acceptor ratios were roughly estimated to be between 1:10 and 1:20 in preliminary experiments by empirically measuring receptor-mediated responses, and occasionally re-titrated due to minor changes in experimental conditions like batch of plasmid preparations or transfection reagents. When included, 0.2 μg of plasmid DNA were transfected for Gβ1 and Gγ2. For experiments with bi-molecular Gβγ biosensors (Figure 2; Figure S1E), cells were transfected as follows: 0.5-1 μg for Gαi3, Gαq, Gαs, or Gαo, 0.2 μg for VC-Gβ1 and VN-Gγ2, and 0.2 μg of mas-GRK3ct-Nluc. For experiments shown in Figure 2 and Figure S1D, cells were transfected with 3 μg for Lyn11-FRB and 0.1 μg for FKBP-R12-GoLoco or 0.05 μg for Ric-8A plasmids in addition to the rest of the BRET biosensor components and GPCRs. For experiments with unimolecular BERKY biosensors (Figures 3 and 6; Figure S2), HEK293T cells were transfected with 0.1-0.2 μg of plasmid DNA per well for Gαi*-BERKY1, Gαi*-BERKY2, Gαi*-BERKY3, KB-1746-BERKY3, Gαq*-BERKY3, Gα13*-BERKY3 or Gβγ-BERKY3. For experiments with Rho*-BERKY3, cells were transfected with 0.025 μg of plasmid DNA per well. When included, 0.2 μg of plasmid DNA were transfected for Gβ1 and Gγ2, and 1 μg for Gαi3, Gαi3 C351I, Gαo, Gαq or Gα13, except in Figure S2F, for which different amounts of Gαi3 were transfected as indicated. The amount for all GPCR plasmid constructs was 0.2 μg per well.

Approximately 18-24 h after transfection, cells were washed with PBS, harvested by gentle scraping, and centrifuged for 5 min at 550 x g. Cells were resuspended in assay buffer (140 mM NaCl, 5 mM KCl, 1 mM $MgCl_2$, 1 mM $CaCl_2$, 0.37 mM NaH_2PO_4, 20 mM HEPES pH 7.4, 0.1% glucose) at a concentration of 1 million cells/ml. 25,000-50,000 cells were added to a white opaque 96-well plate

(Opti-Plate, Perkin Elmer) and mixed with the nanoluciferase substrate Nano-Glo (Promega cat# N1120, final dilution 1:200) for 2 min before measuring luminescence signals in a POLARstar OMEGA plate reader (BMG Labtech) at 28°C. Luminescence was measured at 460 ± 40 nm and 535 ± 10 nm, and BRET was calculated as the ratio between the emission intensity at 535 ± 10 nm divided by the emission intensity at 460 ± 40 nm. For kinetic BRET measurements, luminescence signals were measured every 0.24 s for the duration of the experiment, except for experiments in Figure 2D, and Figures S2E–S2G to determine G-protein activation kinetics, in which measurements were done every 0.04 s. Reagents were added to the wells during live measurements using injectors. BRET data are presented as the difference from baseline BRET signal (average of 30 s pre-stimulation). For experiments with Rho*-BERKY3 (Figure 6D), BRET measurements were carried out with adherent cells by carrying out the modified protocol described next. The day after transfection 12,500-25,000 cells were re-seeded on white opaque 96-well plates coated with 0.1% gelatin, in the presence of DMEM supplemented with 10% FBS, 100 U/ml penicillin, 100 μg/ml streptomycin, and 1% L-glutamine. After 3 h at 37°C in 5% CO_2, media was changed for assay buffer and incubated under the same conditions for 45 min. Cells were equilibrated to room temperature for 15 min before performing BRET measurements as described above. For calculations of BRET response amplitude determined from kinetic experiments, differences were calculated between the pre-stimulation baseline BRET signal and the maximal activation after agonist stimulation (typically between 60-90 s). For endpoint BRET measurements shown in Figure 5B, and Figure S5B, luminescence was read consecutively three times every 30 s and the resulting BRET ratio (535nm luminescence / 460 nm luminescence) values averaged. BRET measurements in SH-SY5Y stable cell lines (see "Generation of cell lines stably expressing unimolecular biosensors" below) shown in Figure S7 were performed essentially as described above for HEK293T cells, except that cells were seeded on 35 mm plates (~900,000 cells/plate) and harvested after approximately 24 h as described above. At the end of some BRET experiments, a separate aliquot of the same pool of cells used for the luminescence measurements was centrifuged for 1 min at 14,000 x g and pellets stored at −20°C for subsequent immunoblot analysis (see "Protein electrophoresis and Immunoblotting" section below).

In Vitro protein binding assays

Protein-protein binding assays with purified GST-fused constructs and proteins expressed in mammalian cells were performed essentially as previously described (Mazarz et al., 2018b). Approximately two million HEK293T cells were seeded on 100 mm dishes and transfected the following day using the calcium phosphate method with 3 μg of plasmids encoding Gαq-YFP (WT or R247L mutants). Twenty-four hours after transfection, cells were lysed on ice with lysis buffer (20 mM HEPES, pH 7.2, 125 mM K(CH_3COO), 0.4% (v:v) Triton X-100, 1 mM DTT, 10 mM β-glycerophosphate, 30 μM GDP and 0.5 mM Na_3VO_4 supplemented with a protease inhibitor [SigmaFAST, cat# S8830]). For some conditions, the lysis buffer was supplemented with 30 μM $AlCl_3$, 10 mM NaF and 10 mM $MgCl_2$ (AlF_4^- condition). Cell lysates were cleared (14,000 x g, 10 min) and used as the source of soluble protein ligands for immobilized GST-fused proteins in pulldown assays. GST-GAIP purification from BL21(DE3) bacteria was carried out exactly as described previously (Mazarz et al., 2018b). GST-GAIP (7.5 μg per condition) was immobilized on glutathione-agarose beads for 90 min at room temperature in PBS. Beads were washed twice with PBS and resuspended in 400 μl of binding buffer (50 mM Tris-HCl, pH 7.4, 100 mM NaCl, 0.4% (v:v) NP-40, 5 mM EDTA, 30 μM GDP, 2 mM DTT), which in some cases was supplemented with 30 μM $AlCl_3$, 10 mM NaF and 10 mM $MgCl_2$ (AlF_4^- condition). After addition of cleared HEK293T cell lysates (~400 μg of total protein), tubes were incubated 90 minutes at 4°C with constant rotation. Beads were rapidly washed four times with 1 mL of wash buffer (4.3 mM Na_2HPO_4, 1.4 mM KH_2PO_4, pH 7.4, 137 mM NaCl, 2.7 mM KCl, 0.1% (v/v) Tween-20, 30 μM GDP, 5 mM EDTA, 1 mM DTT), which in some cases was supplemented with 30 μM $AlCl_3$, 10 mM NaF and 10 mM $MgCl_2$ (AlF_4^- condition). Resin-bound proteins were eluted with Laemmli sample buffer by incubation at 37°C for 10 min and stored at −20°C for subsequent immunoblot analysis (see "Protein electrophoresis and Immunoblotting" section below).

Serum Response Element (SRE) reporter assays

SRE reporter assays were performed as previously described (Mazarz et al., 2018b) with minor modifications. Briefly, HEK293T cells were seeded on 6-well plates (~350,000 cells per well) and transfected 16-24 h later with plasmids pGL3-SRE.L (0.5 μg; Wells et al., 2001) and pCMV-Beta (0.5 μg), along with plasmids for the expression of Gα13-YFP (WT or mutants, 0.2-0.4 μg per well) using the calcium phosphate method. Approximately 6 h after transfection, media was replaced by DMEM containing 0.5% FBS. 16-24 h after transfection, cells were washed with PBS and harvested by gentle scraping followed by centrifugation. Approximately 80% of the cells from one well were pelleted and stored at −20°C for subsequent immunoblot analysis (see "Protein electrophoresis and Immunoblotting" section below). The remaining 20% of the cells were lysed in 60 μl of lysis buffer (Promega, Cat #E2920) for measurement of firefly luciferase and β-galactosidase activity. Fifty μl of the lysates were transferred to wells of a white 96-well OptiPlate (Perkin-Elmer, cat# 6005290) for the determination of firefly luciferase activity using the Dual-Glo Luciferase Assay System (Promega, Cat# E2920) following the manufacturer's instructions. Five μl of the lysates were transferred to wells of a black 96-well OptiPlate (Perkin-Elmer, cat# 6005270) and incubated with 100 μL of the fluorogenic substrate fluorescein di-β-D-galactopyranoside (FDG) (10 μM diluted in 100 mM sodium phosphate buffer, pH 7.5, 1 mM $MgCl_2$, β-mercaptoethanol)) for the determination of β-galactosidase activity following a previously described protocol (Mazarz et al., 2018a). Briefly, fluorescence (Excitation 485 ± 10 nm; Emission 528 ± 10 nm) was measured in a BioTek Synergy H1 plate reader at 30°C every 2 minutes for 90 minutes, and β-galactosidase activity was determined by the fluorescence signal at a time point within the linear portion of the curve, typically between 40-60 min from the beginning of the measurement. For each sample, luciferase activity was normalized to β-galactosidase activity, and SRE activation

Please cite this article in press as: Maziarz et al., Revealing the Activity of Trimeric G-proteins in Live Cells with a Versatile Biosensor Design, Cell (2020), https://doi.org/10.1016/j.cell.2020.06.020

was calculated as the fold-change of normalized luciferase activity relative to activity of cells expressing a control plasmid (pcDNA3.1).

Generation of cell lines stably expressing unimolecular biosensors

Cell lines stably expressing Gαi*-BERKY3, Gβγ-BERKY3, or Gαq*-BERKY3 were generated by lentiviral transduction following previously described procedures with minor modifications (Leyme et al., 2015). Lentivirus packaging was performed in HEK293T cells by co-transfection of the lentiviral plasmid encoding Gαi*-BERKY3, Gβγ-BERKY3, or Gαq*-BERKY3 (in the pLVX-IRES-Hyg backbone) with the packaging plasmids pSPAX2 (Addgene #12260) and pMD2.G (Addgene #12259) at a 1:1:0.5 ratio. Approximately 6 h after transfection the media was changed, and ~42 h later, lentivirus-containing media were collected, centrifuged at 500 x g for 3 min, and passed through a 0.45 μm PES filter. HeLa cells or SH-SY5Y cells seeded in 6-well plates (~200,000 cells / well) were incubated with the supernatant of Gαi*-BERKY3-, Gβγ-BERKY3-, or Gαq*-BERKY3–packaged lentivirus (mixed 1:1 with fresh media) for 2 days, followed by selection with 200 μg/ml hygromycin. All surviving clones were pooled and maintained in the presence of 100 μg/ml hygromycin.

cAMP measurements

Naive HeLa cells, or HeLa cells stably expressing Gαi*-BERKY3 or Gβγ-BERKY3, were seeded in 6-well plates (~400,000 cells / well). After 16-18 h, cells were washed with PBS, resuspended in assay buffer (140 mM NaCl, 5 mM KCl, 1 mM $MgCl_2$, 1 mM $CaCl_2$, 0.37 mM NaH_2PO_4, 20 mM HEPES pH 7.4, 0.1% glucose), centrifuged for 5 min at 1000 x g, and resuspended at a density of 2 million cells /ml of assay buffer supplemented with 0.1% BSA and 1 mM IBMX. After incubation at room temperature for 15 min, cells were stimulated with forskolin (10 μM) for 5 min followed by treatment with different concentrations (0-3000 nM) of brimonidine for 10 min. cAMP was quantified using the LANCE cAMP kit (PerkinElmer, Cat # AD0262) with modifications. Briefly, cells were lysed with the Detection Buffer provided by the kit, and boiled for 3 min at 95°C. All subsequent steps were carried out at room temperature. Following a centrifugation of 3 min at 5,000 x g to sediment particulate material, aliquots of the supernatant were transferred to duplicate wells of a white flat-bottom 384-well ProxiPlate (Perkin Elmer, cat # 6008280) and incubated with anti-cAMP antibody for 30 min. Then, Eu-W8044-streptavidin and biotin-cAMP tracer were added to the wells and after 1 h incubation TR-FRET was measured in a TECAN Infinite M1000 (excitation 317 nm, emission 620 and 665 nm). For each experiment, cAMP was quantified by comparison to a standard curve prepared in duplicate.

ERK1/2 phosphorylation measurements

Naive HeLa cells, or HeLa cells stably expressing Gαi*-BERKY3 or Gβγ-BERKY3, were seeded in 35 mm plates (~200,000 cells/plate). After 24 h, media was replaced with DMEM containing 0.2% FBS. After 16-18 h, cells were treated with 3 μM brimonidine for 5 or 10 min. Stimulation was stopped by placing the plates on ice, washing rapidly with cold PBS, and adding lysis buffer (20 mM HEPES, pH 7.2, 5 mM $Mg(CH_3COO)_2$, 125 mM $K(CH_3COO)$, 0.4% (v:v) Triton X-100, 1 mM DTT, 10 mM β-glycerophosphate, and 0.5 mM Na_3VO_4 supplemented with a protease inhibitor cocktail [SigmaFAST, cat# S8830]). The same procedure was carried out for untreated cells at time zero to harvest unstimulated controls. Cells in cold lysis buffer were harvested by scraping, transferred to cold microcentrifuge tubes, and the lysates were cleared by centrifugation and subject to SDS-PAGE and immunoblotting as described in "Protein Electrophoresis and Immunoblotting."

Lentiviral transduction of primary cortical neurons

For the transduction of cultured neurons, lentiviruses were concentrated after large scale packaging as described next. HEK293T cells (Lenti-X 293T, Cat# 632180, Takara Bio) were plated in 150 mm diameter dishes (~2.5 million cells / dish) and cultured at 37°C, 5% CO_2 in DMEM supplemented with 10% FBS, 100 U/ml penicillin, 100 μg/ml streptomycin, and 1% L-glutamine. After 16-24 h, cells were co-transfected with plasmids encoding Gαi*-BERKY3, Gαi*-BERKY1, Gβγ-BERKY1, or Gαq*-BERKY1 (27 μg / dish) along with the packaging plasmid psPAX2 (18 μg / dish) and the envelope plasmid pMD2.G (11.25 μg / dish) using the polyethylenimine (PEI) method (Longo et al., 2013) at a 2:1 PEI:DNA ratio. Approximately 16 h after transfection, media was replaced with serum-free media. Lentivirus containing media was collected 24 and 48 h after the initial media change (~70 mL per dish and 4 dishes for each construct). Media was centrifuged for 5 min at 900 x g and filtered through a 0.45 μm sterile PES filter. Filtered media was centrifuged for ~12 h at 17,200 x g at 4°C (Sorvall RC6+, ThermoScientific F12-6x500 LEX rotor) to sediment lentiviral particles. Pellets were washed and gently resuspended in 1 mL of PBS and centrifuged at 50,000 x g for 1 h at 4°C (Beckman Optima MAX-E, TLA-55 rotor). Pellets were resuspended in 500 μl of PBS to obtain concentrated lentiviral stocks that were stored at −80°C in aliquots. Each aliquot was thawed only once for subsequent experiments. Primary cortical neurons were transduced with lentiviruses encoding Gαi*-BERKY3, Gαi*-BERKY1, Gβγ-BERKY1, or Gαq*-BERKY1 on DIV7-8 by replacing one half of the media with complete neural media containing lentivirus (final 1:200 dilution) for 1 h, followed by another replacement of one half of the media with fresh complete neural media. Neurons were cultured as described above until experiments were performed at DIV12-16.

BRET measurements in HeLa cells and mouse cortical neurons

HeLa cells stably expressing Gαi*-BERKY3 or Gβγ-BERKY3 were seeded on poly-L-lysine-coated 5 mm coverslips (~35,000 cells/coverslip) placed on 96-well plates and allowed to grow in complete media for 16-24 h before BRET measurements. For measurements with mouse cortical neurons, coverslips of cells transduced with lentiviruses as described above in the section

Please cite this article in press as: Maziarz et al., Revealing the Activity of Trimeric G-proteins in Live Cells with a Versatile Biosensor Design, Cell (2020), https://doi.org/10.1016/j.cell.2020.06.020

"Lentiviral transduction of primary cortical neurons" were processed on DIV 12-16. For each individual measurement, cells were washed with assay buffer (140 mM NaCl, 5 mM KCl, 1 mM $MgCl_2$, 1 mM $CaCl_2$, 0.37 mM NaH_2PO_4, 20 mM HEPES pH 7.4, 0.1% glucose) and the corresponding coverslip transferred to a new well containing assay buffer for an equilibration incubation of 10-20 min (for HeLa cells) or 2-10 min (for neurons) at room temperature in assay buffer. Then, coverslips were transferred to white opaque 96-well plates containing assay buffer and Nano-Glo (final dilution 1:200), and BRET measurements carried out in a POLARstar OMEGA plate reader (BMG Labtech) at 28°C as described above in the section "Bioluminescence Resonance Energy Transfer (BRET) measurements in HEK293T and SH-SY5Y cells." BRET measurements with transiently transfected HeLa cells in suspension shown in Figure S6A were also performed as described for HEK293T and SH-SY5Y cells, except that cells were transfected with 1 μg of Gαi*-BERKY3 plasmid DNA using Lipofectamine LTX reagent and following the manufacturer's instructions.

Immunofluorescence

SH-SY5Y cells, HeLa cells, or primary cortical neurons grown on glass coverslips were fixed with 4% paraformaldehyde diluted in PBS for 10 min at room temperature. Cells were washed 3 times with PBS, permeabilized for 5 min in PBS containing 0.25% (v/v) Triton X-100, and incubated in blocking solution (5% (v/v) normal goat serum, 0.1% (v/v) Triton X-100 in PBS) for 1 hour. Cells were incubated overnight at 4°C with primary antibody diluted in blocking solution (mouse monoclonal GFP antibody, Santa Cruz, sc-9996, 1:100). Coverslips were washed 3 times with PBS and incubated for 1 hour at room temperature with secondary antibody diluted in blocking solution (goat anti-mouse Alexa Fluor 488, Invitrogen A11017, 1:400). Coverslips were stained with DAPI (1 μg/mL in PBS) for 5 min, washed 3 times in PBS and mounted in ProLong Diamond Antifade (Invitrogen P36965). For experiments with HeLa cells (Figure S6) and SH-SY5Y cells (Figure S7), a Zeiss LSM 700 confocal microscope was used to obtain optical sections of 0.29 μm thickness along the Z axis with a 63X oil-immersion objective (numerical aperture [NA] = 1.4; working distance = 0.19 mm) using the ZEN software. For experiments with primary cortical neurons (Figure 7), images were obtained with a Zeiss AxioObserver D1 widefield microscope with a 100X oil-immersion objective (numerical aperture [NA] = 1.4; working distance = 0.17 mm) using the ZEN software. Images were adjusted for brightness/contrast and assembled for presentation using ImageJ, Photoshop and Illustrator softwares (Adobe).

Protein electrophoresis and immunoblotting

Pellets of HEK293T cells used in BRET or SRE experiments, or HeLa cells used in ERK1/2 phosphorylation experiments, were resuspended on ice with lysis buffer (20 mM HEPES, pH 7.2, 5 mM $Mg(CH_3COO)_2$, 125 mM $K(CH_3COO)$, 0.4% (v:v) Triton X-100, 1 mM DTT, 10 mM β-glycerophosphate, and 0.5 mM Na_3VO_4 supplemented with a protease inhibitor cocktail [SigmaFAST, cat# S8830]). Lysates were cleared by centrifugation (10 min at 14,000 x g, 4°C) and boiled for 5 minutes in Laemmli sample buffer before protein separation by SDS-PAGE and electrophoretic transfer to PVDF membranes for 2 h. For *in vitro* protein-protein binding experiments, membranes were stained with Ponceau S solution (0.1% w/v Ponceau S in 5% v/v acetic acid) and imaged on a flatbed scanner prior to further immunoblotting. PVDF membranes were blocked with PBS supplemented with 5% non-fat dry milk (or 5% BSA for ERK1/2 experiments) for 1 hour, and then incubated sequentially with primary and secondary antibodies. Primary antibody dilutions were as follows: Gαi1/2/3, 1:250; pan-Gβ, 1:250; α-tubulin, 1:2,500; Nluc, 1:1,000 (Hall et al., 2012); Gαo, 1:250; Gαq, 1:1,000; Gαs, 1:250; HA, 1:1,000; GFP, 1:1,000; RFP, 1:1,000; Myc, 1:1,000; pERK1/2 (T202/Y204), 1:1,000; and ERK1/2, 1:100. Two different primary antibodies for Gαi3 were used as follows: Gαi3 (Santa Cruz Biotechnology) was used at 1:250 dilution in Figures 1C and 3B; Gαi3 (Aviva Systems Biology) was used at 1:1,000 dilution in Figures 1E and E, and Figure S2F. Secondary antibodies (goat anti-rabbit conjugated to AlexaFluor 680 (Life Technologies) or goat anti-mouse conjugated to IRDye 800 (LI-COR Biosciences)) were used at 1:10,000. Infrared imaging of immunoblots was performed according to manufacturer's recommendations using an Odyssey infrared imaging system (LI-COR Biosciences). Images were processed using the ImageJ software (NIH) and assembled for presentation using Photoshop and Illustrator software (Adobe).

QUANTIFICATION AND STATISTICAL ANALYSIS

All experiments were performed at least three times, as indicated in the figure legends, and, unless otherwise indicated, they are presented as averages ± the standard error of the mean (SEM). For the sake of clarity, in the presentation of kinetic BRET measurements the SEM is only presented in the positive direction and displayed as bars of a lighter color tone than that of its corresponding data points. For experiments in Figure 3D, and Figures S2E–S2G to determine G-protein activation kinetics, data were fit either to a one-phase exponential ("one-component") or to a two-phase exponential ("two-component") equation in GraphPad Prism using least-squares fit. Related parameters (half-times ($t_{1/2}$), percentage distribution among two components of the fit) and residuals were also determined in GraphPad Prism. EC_{50} values were also determined in GraphPad Prism by fitting dose-dependence responses to a three-parameter sigmoidal curve (assuming a Hill slope of 1). Protein structure images displayed in Figure 5A and Figure S5A were prepared in ICM (Molsoft LLC., San Diego, CA). The data displayed in the lollipop plot of Figure S5A were obtained through cBioportal by querying the term GNA13 on December 31st, 2019 in all the datasets classified as Bladder Urothelial Carcinoma.

CellPress

Supplemental Figures

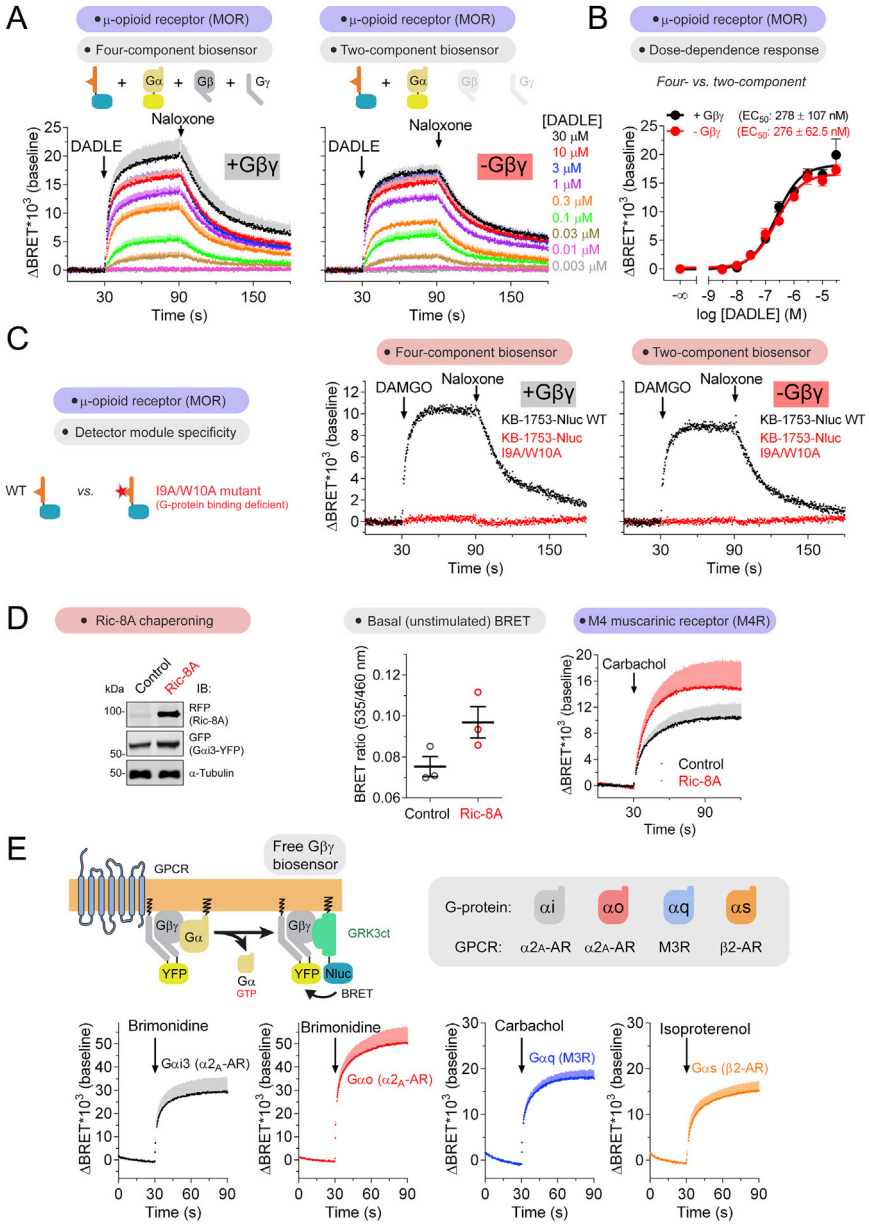

Figure S1. Detection of G-protein Activation by Different GPCRs with Gαi-GTP or Free Gβγ Biosensors and Effect of Ric-8A on Gαi3-YFP, Related to Figure 1

(A and B) Agonist dose-dependent Gαi-GTP responses using four- or two-component biosensors in HEK293T cells expressing MOR. Naloxone = 100 μM. Mean ± S.E.M, n = 3.

(C) Loss of Gαi-GTP response upon mutation of KB-1753-Nluc in HEK293T cells expressing either four- or two-component biosensors. DAMGO = 10 μM; Naloxone = 100 μM. One representative experiment of at least 3.

(D) Co-expression of Ric-8A modestly increases the expression of Gαi3-YFP and enhances BRET signals detected with KB-1753-Nluc with and without GPCR stimulation. BRET measurements were carried out in HEK293T cells with or without GPCR stimulation (M4R, Carbachol = 100 μM) and with or without Ric-8A co-expression. Mean ± S.E.M, n = 3.

(E) *Top:* diagram showing the principle for the free Gβγ biosensor. Upon GPCR stimulation, YFP-tagged Gβγ is relieved from Gα-mediated sequestration, which then permits its association with Nluc-tagged GRK3ct and results in the subsequent increase in BRET. *Bottom:* BRET measurements confirming the release of Gβγ from Gαi, Gαo, Gαq or Gαs. Cells expressing G-proteins with the indicated cognate GPCRs were agonist-stimulated as follows: Gαi3/Gαo, 5 μM brimonidine; Gαq, 100 μM carbachol; Gαs, 10 μM isoproterenol. Mean ± S.E.M, n = 5.

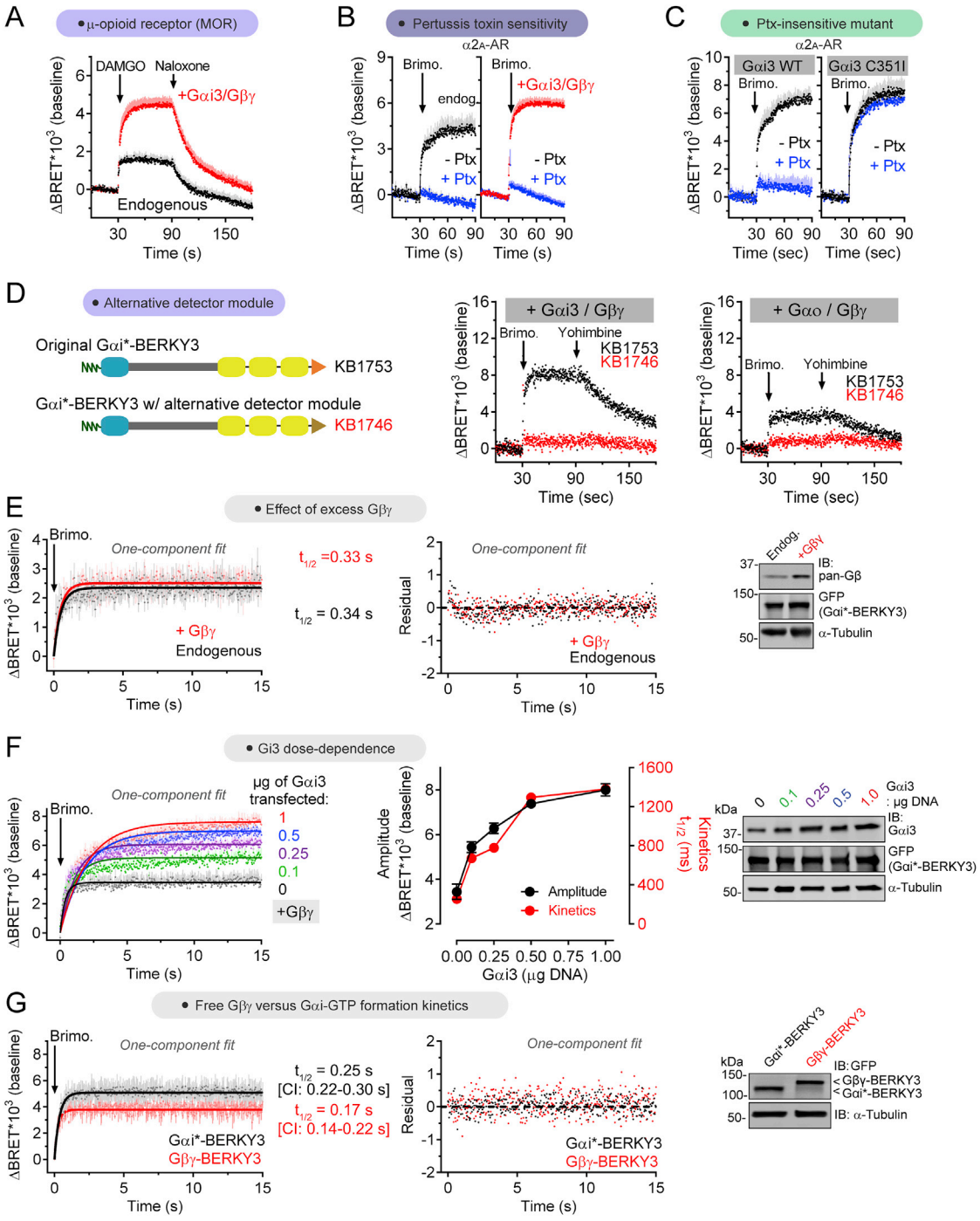

Figure S2. Gαi*-BERKY3 BRET Reports Endogenous Gi Activation upon Stimulation of Different GPCRs, Related to Figure 3

(A) BRET response upon MOR stimulation in HEK293T cells expressing Gαi*-BERKY3 in the absence ("Endogenous") or presence of Gαi3/Gβγ overexpression. DAMGO = 10 μM; Naloxone = 100 μM. Mean ± S.E.M, n = 5.

(B) Pertussis toxin (Ptx) treatment (0.2 μg/ml overnight) abolishes Gαi*-BERKY3 BRET responses detected in HEK293T cells expressing exogenous Gαi3/Gβγ or only endogenous G-proteins upon $\alpha2_A$-AR stimulation (brimonidine, 5 μM). Mean ± S.E.M, n = 3-5.

(C) Pertussis toxin (Ptx) treatment (0.2 μg/ml overnight) does not diminish Gαi*-BERKY3 BRET responses detected in HEK293T cells expressing the Ptx-insensitive mutant Gαi3 C351I upon $\alpha2_A$-AR stimulation (brimonidine, 5 μM). Mean ± S.E.M, n = 3.

(D) BERKY3 biosensors containing the KB-1746 peptide sequence instead of the KB-1753 peptide sequence as detector module fail to detect activation of $G_{i/o}$ proteins. BERKY biosensor designs with different detector modules are shown on the left, and representative traces comparing side by side BRET responses

(legend continued on next page)

detected with each biosensor in HEK293T cells expressing the indicated G-proteins and the $\alpha 2_A$-AR are shown on the right. Brimonidine = 5 μM; Yohimbine = 25 μM.

(E) Endogenous Gαi activation kinetics determined by Gαi*-BERKY3 BRET are not affected by expression of exogenous Gβγ. Gαi activation kinetics were determined in HEK293T cells expressing Gαi*-BERKY3 in the absence and presence of Gβγ overexpression (but no Gα) upon GPCR stimulation ($\alpha 2_A$-AR, 5 μM brimonidine). Data points are mean ± SEM and solid lines are fits to one-component exponential curves (n = 3-4). Residual plot of the curve fit is shown in the middle panel, and a representative immunoblot confirming the expression of different components is shown on the right.

(F) Expression of exogenous Gαi3 alters Gαi activation kinetics and amplitude in a dose-dependent manner as determined by Gαi*-BERKY3 BRET. Gαi activation kinetics were determined in HEK293T cells expressing Gαi*-BERKY3 in presence of different amounts of Gαi3 (as indicated) and constant Gβγ. Data points are mean ± SEM and solid lines are fits to one-component exponential curves (n = 4). Comparison of response amplitude (black) and $t_{1/2}$ (red) for different amounts of Gαi3 is shown in the middle panel, and a representative immunoblot confirming the expression of different components is shown on the right.

(G) Formation of Gα-GTP and formation of free Gβγ proceed with similar kinetics upon GPCR stimulation. Gαi*-BERKY3 or Gβγ-BERKY3 BRET kinetics were determined in HEK293T cells expressing only endogenous G proteins upon GPCR stimulation ($\alpha 2_A$-AR, 5 μM brimonidine). Data points are mean ± SEM and solid lines are fits to one-component exponential curves (n = 3). Residual plot of the curve fit is shown in the middle panel, and a representative immunoblot confirming the expression of different components is shown on the right.

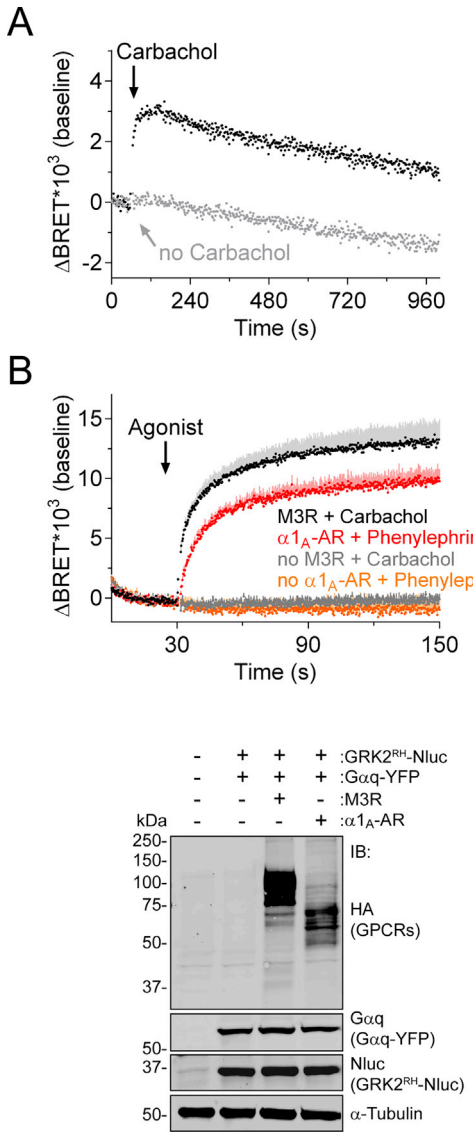

Figure S3. Direct Detection of GTP-Bound Gαq in Cells upon Long-Term Stimulation of the M3R or upon Stimulation of the $\alpha 1_A$-AR, Related to Figure 4

(A) Carbachol stimulation of the M3R leads to a sustained Gαq-GTP BRET response for over 15 minutes. HEK293T cells expressing the M3R and the components of the Gαq-GTP biosensor were stimulated with carbachol (100 μM, black trace) or left unstimulated (gray trace). One representative experiment of two is shown. (B) HEK293T cells expressing the M3R or the $\alpha 1_A$-AR and the components of the Gαq-GTP biosensor were stimulated with carbachol (100 μM) or phenylephrine (10 μM), respectively. Immunoblots on the bottom show the expression of the two GPCRs and different components of the biosensor system. Mean ± S.E.M, n = 3.

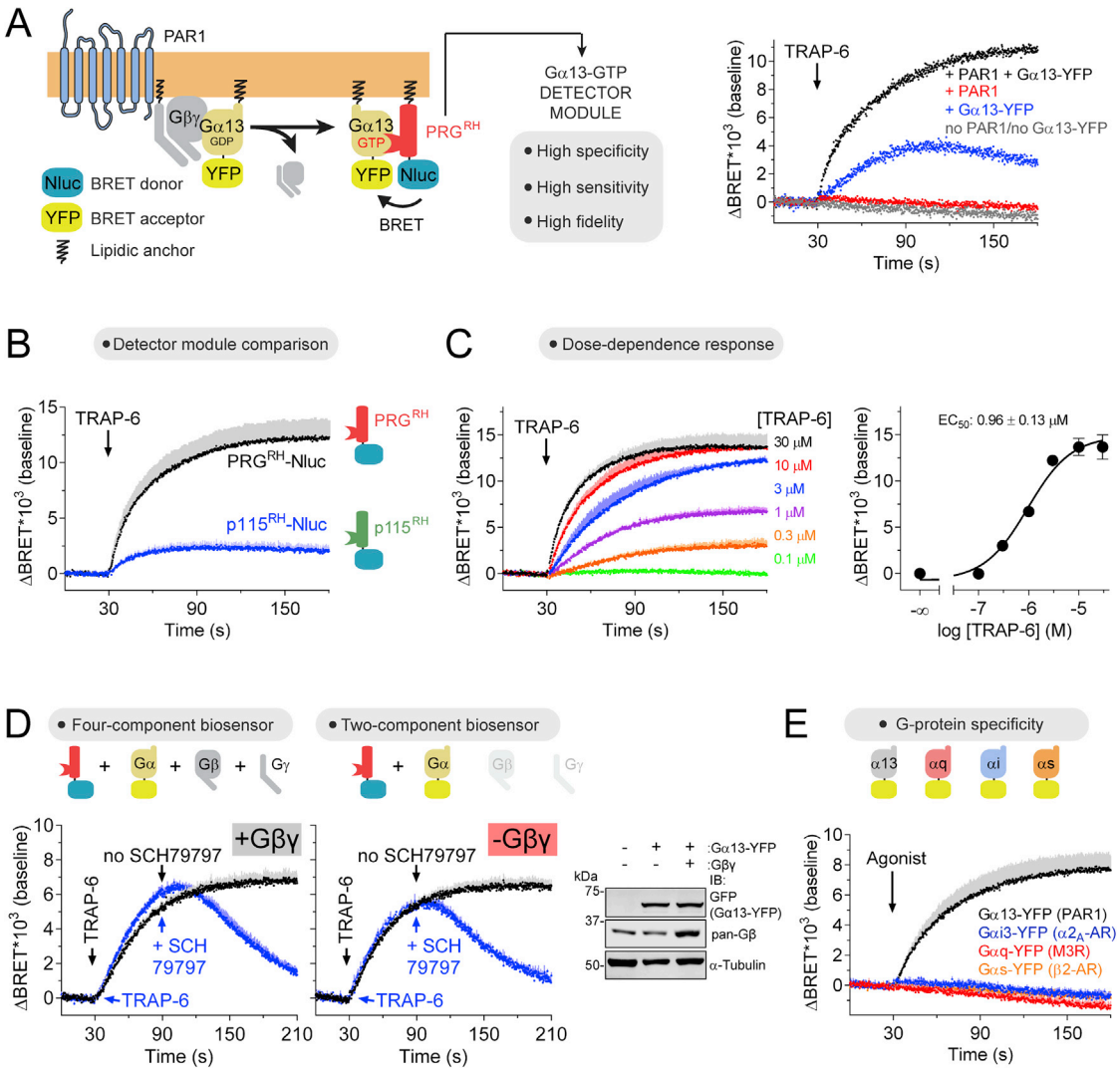

Figure S4. Direct Detection of GTP-Bound Gα13 in Cells, Related to Figure 4

(A) Gα13-GTP biosensor design principle and representative traces of BRET measurements in HEK293T cells expressing PRG^{RH}-Nluc along with the indicated constructs. BRET response in "+Gα13-YFP" condition without exogenous PAR1 expression likely reflects stimulation of endogenous PAR1 receptors, as previously reported by others with another biosensor of Gα13 activity using the same cell line (PMID: 26628681). TRAP-6 = 30 μM.

(B) PRG^{RH}-Nluc biosensor detects more robust Gα13 BRET responses than p115^{RH}-Nluc in HEK293T cells expressing exogenous PAR1. TRAP-6 = 30 μM. Mean ± S.E.M, n = 3.

(C) PRG^{RH}-Nluc biosensor detects agonist dose-dependent Gα13-GTP responses in HEK293T cells expressing PAR1. Mean ± S.E.M, n = 3.

(D) Gα13-GTP BRET responses are reversible and can be detected similarly with either four- or two-component biosensors. HEK293T cells expressing the PAR1 and the indicated components of PRG^{RH}-Nluc biosensors were stimulated with TRAP-6 (1 μM) and in some cases (blue traces) subsequently treated with the antagonist SCH-79797 (10 μM). Mean ± S.E.M, n = 3-4.

(E) Detection of Gα13-GTP but not Gαq-GTP, Gαi3-GTP or Gαs-GTP responses by PRG^{RH}-Nluc upon GPCR agonist stimulation. Cells expressing G-proteins with the indicated cognate GPCRs were agonist-stimulated as follows: Gα13, 10 μM TRAP-6; Gαq, 100 μM carbachol; Gαi3, 10 μM brimonidine; Gαs, 10 μM isoproterenol. Mean ± S.E.M, n = 3.

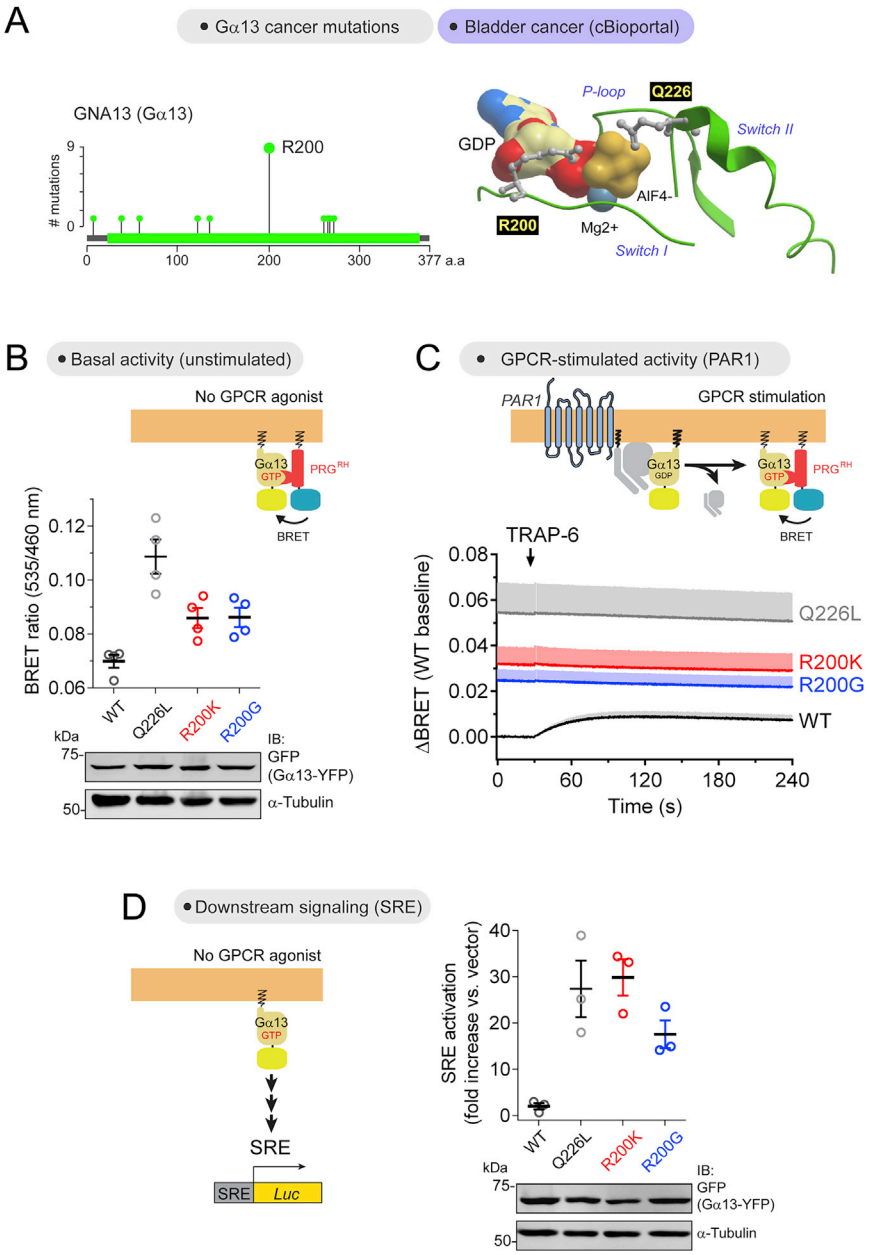

Figure S5. Characterization of Cancer-Associated G-protein Mutants with a Gα13-GTP Biosensor, Related to Figure 5

(A) Lollipop plot of Gα13 residues mutated in bladder cancer and three dimensional model of Gα13 (PDB: 3AB3) showing the position of selected residues around the nucleotide binding site.

(B) Cancer-associated Gα13 mutants R200K and R200G are constitutively active as determined by the Gα13-GTP biosensor PRG^{RH}-Nluc in HEK293T cells. Mean ± S.E.M, n = 4.

(C) Stimulation of exogenously expressed PAR1 activates Gα13 WT but not Gα13 mutants R200K and R200G as determined by the Gα13-GTP biosensor PRG^{RH}-Nluc in HEK293T cells. Mean ± S.E.M, n = 3.

(D) Cancer-associated Gα13 mutants R200K and R200G are constitutively active as determined by a luciferase reporter of a modified Serum Response Element (SRE) in HEK293T cells. Mean ± S.E.M, n = 3.

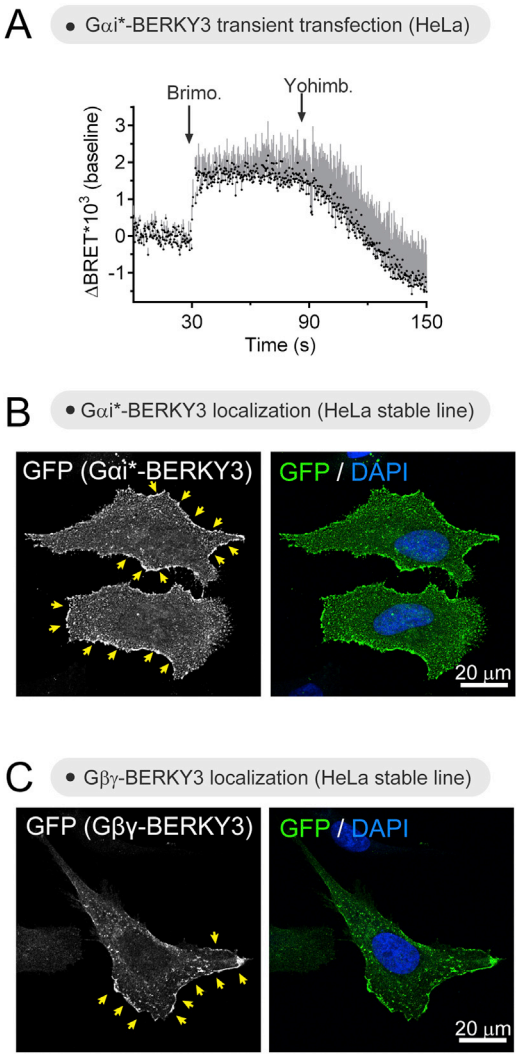

Figure S6. Gαi*-BERKY3 BRET Response in Transiently Transfected HeLa Cells and Cellular Localization of Gαi*-BERKY3 and Gβγ-BERKY3 Biosensors Expressed in HeLa Cells, Related to Figure 7

(A) Transiently transfected Gαi*-BERKY3 detects endogenous G-protein activation by endogenous α2-AR in HeLa. HeLa cells were harvested 24 hours after transfection and rapidly assayed in suspension. Brimonidine = 5 μM; Yohimbine = 25 μM. Mean ± S.E.M, n = 3.

(B and C) HeLa cell lines stably expressing Gαi*-BERKY3 or Gβγ-BERKY3 biosensors generated as depicted in Figure 7A were imaged by confocal immunofluorescence microscopy. Arrowheads indicate accumulation of signal at the cell periphery, presumably the cell membrane.

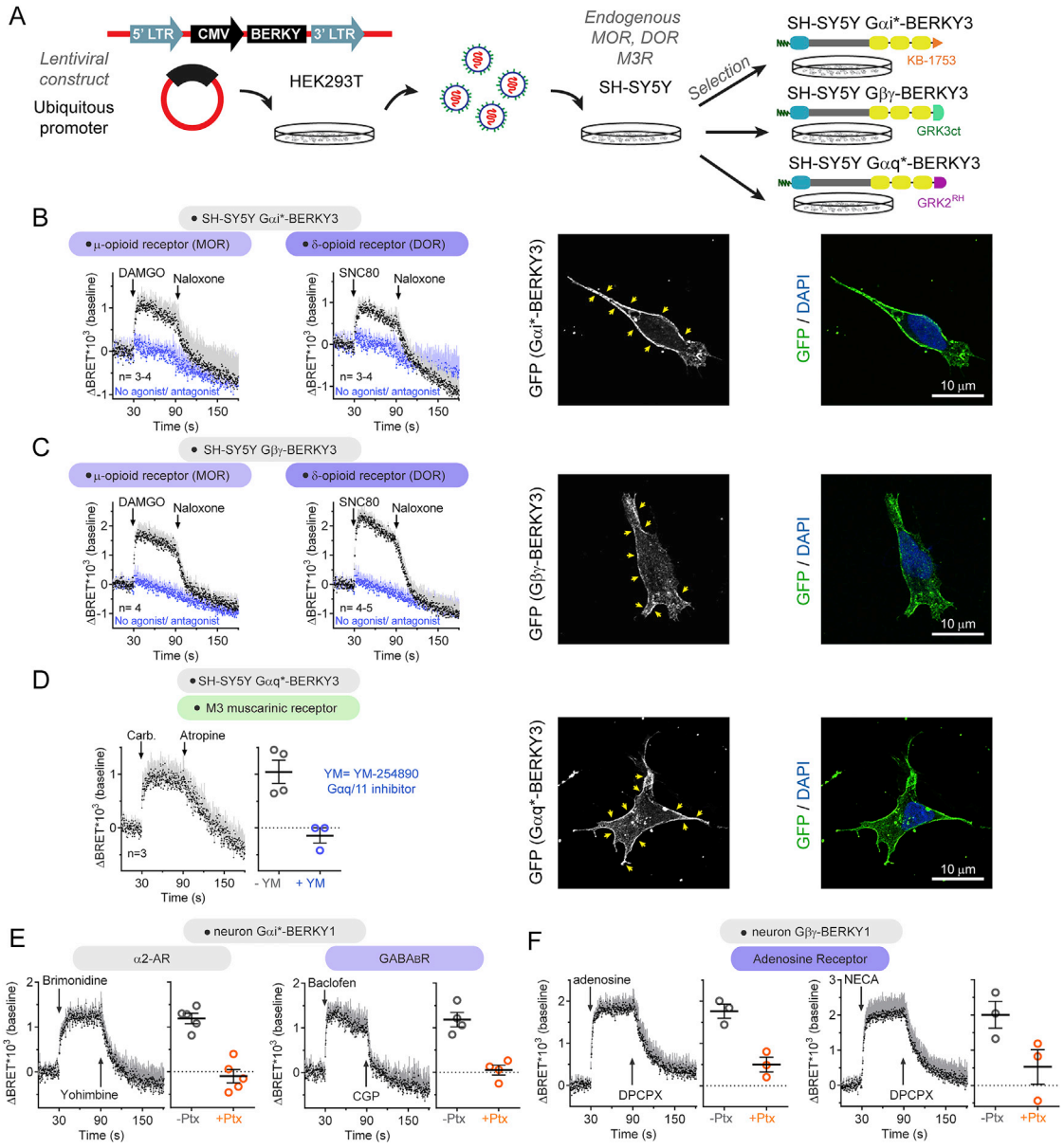

Figure S7. Detection of Endogenous G-protein Activation by Multiple Endogenous GPCRs in SH-SY5Y Cells and Primary Neurons, Related to Figure 7

(A) Generation of SH-SY5Y cell lines stably expressing Gαi*-BERKY3, Gβγ-BERKY3 or Gαq*-BERKY3 to monitor G-protein activation upon stimulation of endogenously expressed MOR, DOR, or M3R.

(B–D) Endogenous Gαi-GTP (in (B), free Gβγ (in (C), or Gαq-GTP (in (D) BRET responses detected by BERKY biosensors upon stimulation of endogenous GPCRs in SH-SY5Y cells. Mean ± SEM of the number of experiments (n) indicated in the figures. DAMGO = 1 μM; SNC80 = 10 μM; Naloxone = 100 μM; Carbachol = 1 mM; Atropine = 100 μM; YM-254890 = 10 μM (10 min preincubation). Confocal immunofluorescence images of representative cells expressing BERKY biosensors are shown on the right. Arrowheads indicate accumulation of signal at the cell periphery, presumably the cell membrane.

(E and F) Endogenous Gαi-GTP (in (E) or endogenous free Gβγ (in (F) BRET responses detected upon stimulation of endogenous GPCRs in primary cortical neurons (DIV 12-16) transduced with Gαi*-BERKY1 or Gβγ-BERKY1, respectively. Responses to α2-AR (brimonidine, 5 μM), $GABA_BR$ (baclofen, 100 μM) or adenosine receptors (adenosine, 10 μM; NECA, 10 μM) are blocked by pertussis toxin (Ptx, 0.2 μg/ml overnight preincubation). Yohimbine = 25 μM; CGP 54626 (CGP) = 10 μM; DPCPX = 1 μM. Mean ± S.E.M., n = 3-5.